

1 **A study of the combined impact of boundary layer height and near-surface meteorology to the CO**
2 **diurnal cycle at a low mountaintop site using simultaneous lidar and in-situ observations**

3 S. Pal ^{1,2,*}, T. R. Lee ^{1,3}, and S. F. J. De Wekker ¹

4 ¹ Department of Environmental Sciences, University of Virginia, Charlottesville, VA, USA

5 ² Now at Department of Meteorology and Atmospheric Science, The Pennsylvania State
6 University, University Park, PA, USA

7 ³ Now at Oak Ridge Associated Universities and NOAA ARL Atmospheric Turbulence and
8 Diffusion Division, Oak Ridge, TN, USA

9 **Type:** Research Paper

10 **Journal:** Atmospheric Environment

11 **Revised version submitted on May 19, 2017.**

12

13

14 ***Corresponding author:**

15 Dr. S. Pal

16 Department of Environmental Sciences, University of Virginia

17 291 McCormick Rd., Charlottesville

18 VA 22904-4123, USA

19 E-Mail: sup252@psu.edu; pal_sandy2002@yahoo.co.uk

20 Phone: +1 434-326-7706

21 **Keywords:** Air pollution; Carbon monoxide; Convective boundary layer height, Lidar;
22 Mountaintop; Upslope flow.

23 **Abstract**

24 Evaluations of air pollutants and trace gas measurements over mountaintop sites and their
25 application in inverse transport models to estimate regional scale fluxes are oftentimes
26 challenging due to the influences associated with atmospheric transport at both local and regional
27 scales. The objective of this study is to investigate the diurnal cycle pattern of CO mixing ratio
28 over a low mountaintop influenced by: (1) two different convective boundary layer (CBL)
29 regimes (shallow and deep) and associated growth rates over the mountaintop, (2) the combined
30 effect of a deep CBL with and without diurnal wind shift, and (3) slope flows and associated air
31 mass transport. For this purpose, we used simultaneous measurements of lidar-derived CBL
32 heights, standard meteorological variables, and CO₂ and CO mixing ratio from Pinnacles, a
33 mountaintop monitoring site in the Appalachian Mountains. We used both water vapor and CO₂
34 mixing ratio as tracers for upslope flow air masses. We used case studies to focus on two
35 different scenarios of daytime CO mixing ratio variability: (1) a gradual increase in the morning
36 with a maximum in the afternoon, and (2) a gradual decrease in the morning with a minimum in
37 the late afternoon. The second scenario is similar to the CO variability observed atop tall towers
38 in flat terrain.

39 Using the lidar-derived CBL height evolution and in situ CO, CO₂ and meteorological
40 measurements over the mountaintop, we found that the upslope flow air masses arriving at the
41 mountaintop in the morning affect the CO mixing ratio variability during the remaining part of
42 the diurnal cycle. These findings help introduce a conceptual framework that can explain and
43 differentiate the opposite patterns (i.e. daytime increase versus daytime decrease) in the CO
44 diurnal cycles over a mountaintop site affected by upslope flows and provide new roadmaps for

45 monitoring and assimilating trace gas mixing ratios into applications requiring regionally-
46 representative measurements.

47 **1. Introduction**

48 Trace gas measurements at mountaintop locations are valuable as they help determine
49 background mixing ratios in the free atmosphere (FA) which are important for studies of long-
50 range impacts of upwind source regions. However, greenhouse gases (GHG) such as carbon
51 dioxide (CO₂) and trace gases such as carbon monoxide (CO) and O₃ are affected by site-specific
52 meteorological conditions in mountainous terrain (e.g., Schmitt and Volz-Thomas, 1997; Lee et
53 al., 2015; Sullivan et al., 2017), synoptic scale transport, e.g., via frontal passages (e.g., Pillai et
54 al., 2011), and thermally driven recirculation pattern in the mountain-valley atmosphere (e.g., De
55 Wekker et al., 2009; Sullivan et al., 2016). Additionally, air pollutants in mountainous areas
56 include harmful airborne substances that threaten human health, harm vegetation, animals or
57 structures, or affect visibility (Whiteman, 2000). However, our knowledge of the effect of
58 complex terrain on air pollution in mountainous areas remains limited due to sparse observations
59 (Lee, 2015) and to difficulties with numerical simulations in these areas (e.g., Desai et al., 2010;
60 Steyn et al., 2012; Lin et al., 2016).

61 In mountainous regions, terrain-induced atmospheric processes can influence the diurnal cycle of
62 trace gas mixing ratios. For example, flows along the valley and slopes are generated due to
63 horizontal temperature gradients arising from heating and cooling of valley atmospheres and the
64 atmosphere adjacent to sloping terrain. These flows are directed upvalley and upslope during
65 daytime and downvalley and downslope at night (e.g., Whiteman, 2000). The mountaintop
66 measurements of CO, CO₂, O₃, water vapor, aerosols, and other tracers are influenced by these

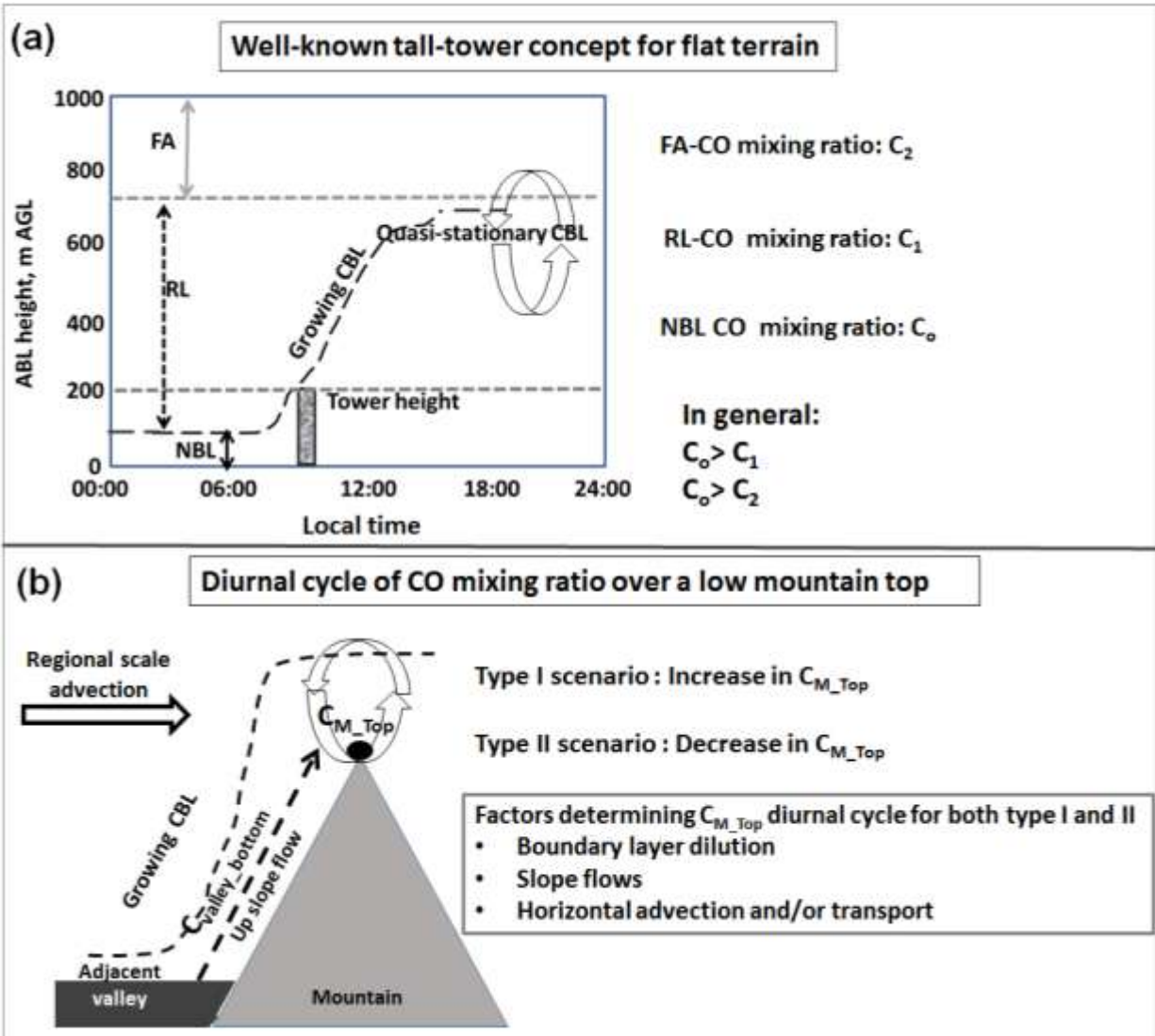
67 flows, i.e. upslope flows bring air from the adjacent lowland boundary layer up to the summits
68 (e.g., Fischer et al., 2004). Several investigators (e.g., Keeling et al., 1976; De Wekker et al.,
69 2009) found that CO₂ mixing ratio time series exhibited a pronounced afternoon minimum in
70 summer, which they partly attributed to the transport of CO₂ depleted air via upslope flows.
71 Understanding these influences is important to better estimate the regional scale fluxes of CO₂
72 where CO is used to distinguish anthropogenic CO₂ from biogenic CO₂ (e.g., Andrews et al.,
73 2014).

74 Previous studies focusing on CO and CO₂ mixing ratio variability over high-altitude sites,
75 including Jungfraujoch (~ 3500 m mean sea level (MSL)) in the Swiss Alps (e.g., Dils et al.,
76 2011), Nainital (~ 2000 m MSL) in the central Himalayas (e.g., Sarangi et al., 2014) and Mauna
77 Loa (3397 m MSL) in Hawaii (e.g., Atlas and Ridley, 1996), illustrate that these sites mostly
78 sample free atmospheric (FA) air except on days when the convective boundary layer (CBL)
79 height is relatively large. The CO mixing ratio oftentimes reaches a maximum in the late
80 afternoon hours (e.g., ~18:00 LST) due to the impact of upslope flows bringing polluted air from
81 the adjacent valleys and plains (e.g., Dils et al., 2011). For low mountaintop sites like
82 Ochsenkopf (1022 m MSL, situated in the Fichtelgebirge mountain range in Germany), the
83 impact of upslope flow on the tracer mixing ratios is common throughout the year except in
84 winter (Pillai et al., 2011). However, the role of CBL height variability over the mountaintop on
85 CO mixing ratios on diurnal time scale has not been properly addressed using observational
86 findings. Only recently have researchers emphasized a conceptual framework to illustrate CO
87 diurnal cycle pattern over mountaintop sites (e.g., Bamberger et al., 2014, 2017; Lin et al., 2016)
88 as was performed for CO₂ diurnal pattern over flat terrain (e.g., Pino et al., 2012; Haszpra et al.,
89 2015).

90 Complex meteorology and lack of observations are important hurdles to study exchange
91 processes in a mountain-valley atmosphere system. Empirical work illustrating the combined
92 impacts of both meteorology and CBL height variability and relevant dynamics on the CO
93 diurnal cycle is very limited. While several studies report CO variability on diurnal, synoptic and
94 seasonal time scales, we are unaware of studies that demonstrate specifically the importance of
95 continuously monitored mountaintop CBL heights on CO variability. Furthermore, the driving
96 factors that yield contrasting patterns (i.e. daytime increase versus daytime decrease) in the
97 diurnal cycles of trace gases, including CO, have so far not been explained. In this work, we
98 emphasize a process-based framework by investigating CO mixing ratio measurements on a
99 mountaintop monitoring site in the Blue Ridge Mountains in northwestern Virginia that we refer
100 to as Pinnacles, (38.61 N, 78.35 W, 1017 m MSL). The objective of this study is to investigate
101 diurnal CO patterns influenced by (1) daytime CBL height variability and growth rate, (2) the
102 slope wind system in the mountain-valley atmosphere, and (3) prevailing synoptic settings
103 including on site meteorological conditions, in particular, a horizontal wind shift. We use
104 continuous high-resolution lidar measurements at Pinnacles to investigate the CBL height
105 variability during four selected days. CO and CO₂ measurements and other meteorological
106 measurements were collected from a 17 m walkup tower that was established at Pinnacles in
107 May 2008.

108 **2. Basic concept and hypothesis**

109 Based on the previous studies on trace gas measurements over complex terrain, we consider CO
110 mixing ratios to be a good proxy for boundary layer mixing processes. Figure 1 presents a
111 conceptual framework for the general mechanisms governing the CO diurnal cycle on a tall
112 tower located in flat terrain and on a low mountaintop site. During the morning transition period,



113

114 **Fig. 1.** Schematics of the general mechanisms governing the diurnal cycle variability of CO
 115 mixing ratio on a tall tower in flat terrain (a) and on a low mountaintop site (b). NBL, RL, and
 116 FA denote the nocturnal boundary layer, residual layer, and free atmosphere, respectively. CO ,
 117 C_1 , and C_2 denote CO mixing ratios in the NBL, RL, and FA, respectively. In the top figure,
 118 horizontal dashed lines mark the levels of the tower top and of the quasi-stationary height of
 119 daytime well-mixed CBL and vertically-aligned arrows mark the NBL, RL and FA. The curved
 120 dashed line and thick circular arrows in both figures illustrates the growing CBL and
 121 entrainment mixing at the CBL top, respectively. CO mixing ratios at the valley and at the
 122 mountaintop site just before sunrise are referred to as C_{valley_bottom} and C_{M_Top} , respectively. The
 123 diurnal cycle of C_{M_Top} responds to the CBL dynamical processes, in particular, CBL height and
 124 air mass from adjacent valley transported via upslope flow. Type I and II scenarios refer to
 125 increase and decrease of C_{M_Top} , respectively due to the combined impact of boundary layer
 126 dilution, slope flows (dashed arrow aligned along the mountain slope) and regional scale
 127 advection (horizontally aligned thick arrow).

128 polluted nocturnal boundary layer (NBL) air reaches the tower top, illustrating a morning peak in
129 the CO mixing ratio variability. After the CBL begins growing, the CO mixing ratio at the tower
130 top starts decreasing under the assumption that CO mixing ratio is higher in the NBL than in the
131 residual layer (RL); CO continues to decrease due to the dilution effect until the late afternoon
132 hours when the CBL attains a quasi-stationary state, yielding a daytime minimum mixing ratio
133 until the evening transition period when the NBL starts developing.

134 Similar to the CO diurnal cycle on a tall tower, mountaintop measurements are also affected by
135 the CBL dilution effect via boundary layer growth and by horizontal advection. Additionally,
136 vertical transport by upslope flow affects mountaintop trace gas measurements in mountainous
137 regions and causes a daytime peak in the CO mixing ratio which is similar to the arrival of NBL
138 air reaching the tall tower top during the morning transition. During nighttime, the top of a tall
139 tower usually remains either in the RL or in the NBL depending on the NBL height. In contrast,
140 mountaintops generally sample either FA or RL air depending on the daytime CBL height
141 variability. This is because of the subsiding motions generated by downslope flows at the
142 mountaintop that transport FA air to mountaintop level (e.g., Pillai et al., 2011). Therefore, a
143 traditional NBL does not develop over a mountaintop and instead nighttime mountaintop
144 measurements are considered representative of FA or RL measurements (Whiteman, 2000).

145 Nevertheless, we hypothesize that the tall tower concept can be applied to explain the CO mixing
146 ratio variability over a mountaintop site under certain conditions that require knowledge of the
147 CBL height diurnal cycle at the mountaintop location. Additionally, for flat terrain, Pino et al.
148 (2012) outlined the importance of considering near-surface CO₂ mixing ratios in the early
149 morning to interpret the observed CO₂ variability during the afternoon over flat terrain.
150 Similarly, the CO variability during the morning transition period at low mountaintops also

151 depends on the nighttime CO mixing ratios at the site before the arrival of adjacent valley air. In
152 this context, low mountaintop sites refer to the ridges that are located around 500-1000 m above
153 adjacent valleys or plains and include, e.g., Ochsenkopf (1022 m MSL, a monitoring station in
154 the Fichtelgebirge Mountains of northern Bavaria in Germany) (e.g., Thompson et al., 2009),
155 Hornisgrinde (1161 m MSL) in the Black Forest of Germany (Vöglin et al., 1996), and
156 Pinnacles in the Appalachian Mountains of the eastern US (e.g., Lee et al., 2012), the site we
157 focus on in the current study.

158 Figure 1 illustrates that during the morning transition period, the valley air with $C_{\text{valley_bottom}}$
159 reaches the mountaintop and mixes with the air with $C_{\text{M_Top}}$. In general, $C_{\text{M_Top}}$ measurements in
160 the morning before upslope flow arrives at the site help identify NBL-CO mixing ratio and
161 determine which layer (RL or FA) of the atmosphere is being sampled. It is therefore considered
162 a quantifiable tracer of the atmospheric dynamics occurring in the mountain-valley atmosphere.
163 We consider two types of diurnal scenarios affected by mountaintop meteorological conditions
164 and CBL regime: (1) daytime increase in $C_{\text{M_Top}}$ (type I scenario resembling NBL air reaching
165 tall tower top in the morning), and (2) a decrease in $C_{\text{M_Top}}$ (type II scenario resembling CBL
166 dilution effect in flat terrain). Additionally, we also hypothesize that, $C_{\text{M_Top}}$ during type I and II
167 scenarios is influenced by the combined effect of (1) local meteorological conditions, (2) arrival
168 of different air masses at the mountaintop via either upslope flow or horizontal transport, and
169 finally (3) CBL height and growth rate. In this paper, we use some case studies to illustrate the
170 processes playing a dominant role in governing the CO diurnal cycle for both type I and II
171 scenarios.

172

173 3. Experimental site, instruments and data sets

174 The data sets were collected on a 17 m walkup tower located at Pinnacles, a forested
175 mountaintop site in the Shenandoah National Park (SNP) of the Blue Ridge Mountains of
176 Virginia. The research station at Pinnacles was established in May 2008 along a ridgeline at an
177 elevation of 1017 m (38.61°N, 78.35°W) in the north-central section of SNP. Further details on
178 the infrastructure of the Pinnacles station, geography, and climatology of the region are reported
179 in Lee et al. (2012, 2015).

180 The tower is outfitted with a suite of instruments, including meteorological sensors and
181 micrometeorological instruments, a Thermo Electron 48C Trace Level CO Analyzer for
182 measuring CO mixing ratios at three levels (5, 10, 17 m above ground level (AGL)), and a Li-
183 COR 7000 closed path gas analyzer for CO₂ mixing ratios at these same three levels (e.g., Lee et
184 al., 2012; Andrews et al., 2014). The meteorological sensors include a Campbell Scientific 3D
185 Sonic anemometer (CSAT3) combined with LI-COR 7500 open-path gas analyzer for CO₂,
186 latent, and sensible heat fluxes, Hukseflux four-component net-radiation sensor for incoming and
187 outgoing short- and long wave radiation, MetOne 034B cup and vane anemometer for horizontal
188 wind speed and direction, Vaisala HMP45 probe for humidity and temperature, a Vaisala CS105
189 for pressure, and a TR-525I tipping bucket rain gauge. For each collected variable, a set of
190 quality assurance and quality control procedures was implemented. More detailed information
191 about the trace gas and meteorological data sets, as well as the quality control algorithms
192 implemented, can be found in Lee (2015).

193 When CBL height measurements over mountaintop sites are concerned, previous studies mainly
194 used maximum CBL height derived from nearby rawinsonde profiles (Lee and De Wekker,

2016), from numerical model simulations (e.g., Pillai et al., 2011), from lidar measurements in
an adjacent valley (e.g., Gallagher et al. 2012), or from combined lidar and radar observations
from adjacent plains (e.g., Sullivan et al., 2016). However, the potential of continuous
monitoring of CBL height using ground-based profilers (e.g., lidar, radar, sodar, wind profiler)
over mountaintop sites for elucidating the CO diurnal cycle characteristics has not been
addressed. At Pinnacles, a Leosphere ALS-300 eye-safe aerosol lidar was occasionally deployed
at the site for monitoring CBL height over the region. The lidar system installed at the site
operates at a wavelength of 355 nm (UV range) and provides profiles of relative particle
backscatter at temporal and vertical resolutions of 1 minute and 15m, respectively. During post-
processing, profiles of range-squared corrected backscatter signal intensities were used to
estimate CBL heights by applying the Haar wavelet algorithm (Pal et al., 2014, 2015).

Using aerosols as tracers for CBL mixing processes, the Haar wavelet algorithm has been used
for nearly two decades to estimate CBL height from aerosol lidar observations (e.g., Cohn and
Angevine, 2000; Pal et al., 2009, 2015). Based on a sensitivity test that is typically done for Haar
wavelet method, we used a dilation of 150 m for the analysis; the time resolution between two
profiles is 1 minute, and the range resolution in the backscatter data is 15 m. The dilation value
depends on several factors: (1) temporal and spatial resolution of the lidar signal profiles, (2)
signal to noise ratio; (3) atmospheric conditions revealing particle backscatter strengths, and (4)
limit of wavelet covariance transform integration. We tested various dilations (a in the wavelet
transformation equation, see e.g Cohn and Angevine, 2000; Pal et al., 2010) and found 150 m to
be appropriate where multiple peaks in the wavelet coefficients were absent yielding the most
appropriate location of maximum gradient in altitude, i.e. top of the CBL. For further discussion

217 on the wavelet application for determining CBL heights, readers are referred to Davis et al.
218 (2000) and Pal et al. (2010).

219 In this study, we use lidar measurements collected on selected clear sky days in 2009 to
220 investigate the impact of CBL height on the CO mixing ratio variability on a diurnal time scale.
221 Full overlap of the transceiver of the lidar system is attained at a height of ~ 200 m AGL, and
222 thus estimates of CBL height below this height cannot be made with the lidar system (e.g.,
223 Behrendt et al., 2005; Pal, 2014).

224 **4. Meteorological conditions**

225 An overview of the near-surface meteorological conditions is presented in Table 1, which reports
226 the daily maximum, minimum temperature, diurnal temperature range, clearness index based on
227 the incoming solar radiation (Whiteman et al., 1999), regimes of diurnal wind shift, and times of
228 sunrise and crossover of sensible heat fluxes (SHF) (i.e., the time when sensible heat flux
229 changes sign). A clearness index of more than 0.6 was observed at the site on all the days
230 confirming the absence of significant cloud cover during the daytime (Table 1).

231 For obtaining a general overview on the prevailing synoptic settings for those case studies, we
232 used 3-hourly surface reanalysis charts produced by NOAA-HPC. Prevailing synoptic conditions
233 on all four selected days of interest were characterized by near-surface anti-cyclonic flow in the
234 region around Pinnacles (Fig. 2). In particular, on 21 May and 21 October 2009, there was an
235 anti-cyclone located over the Mid-Atlantic; on 5 and 14 September 2009, the anti-cyclone was
236 positioned over the upper Midwest.

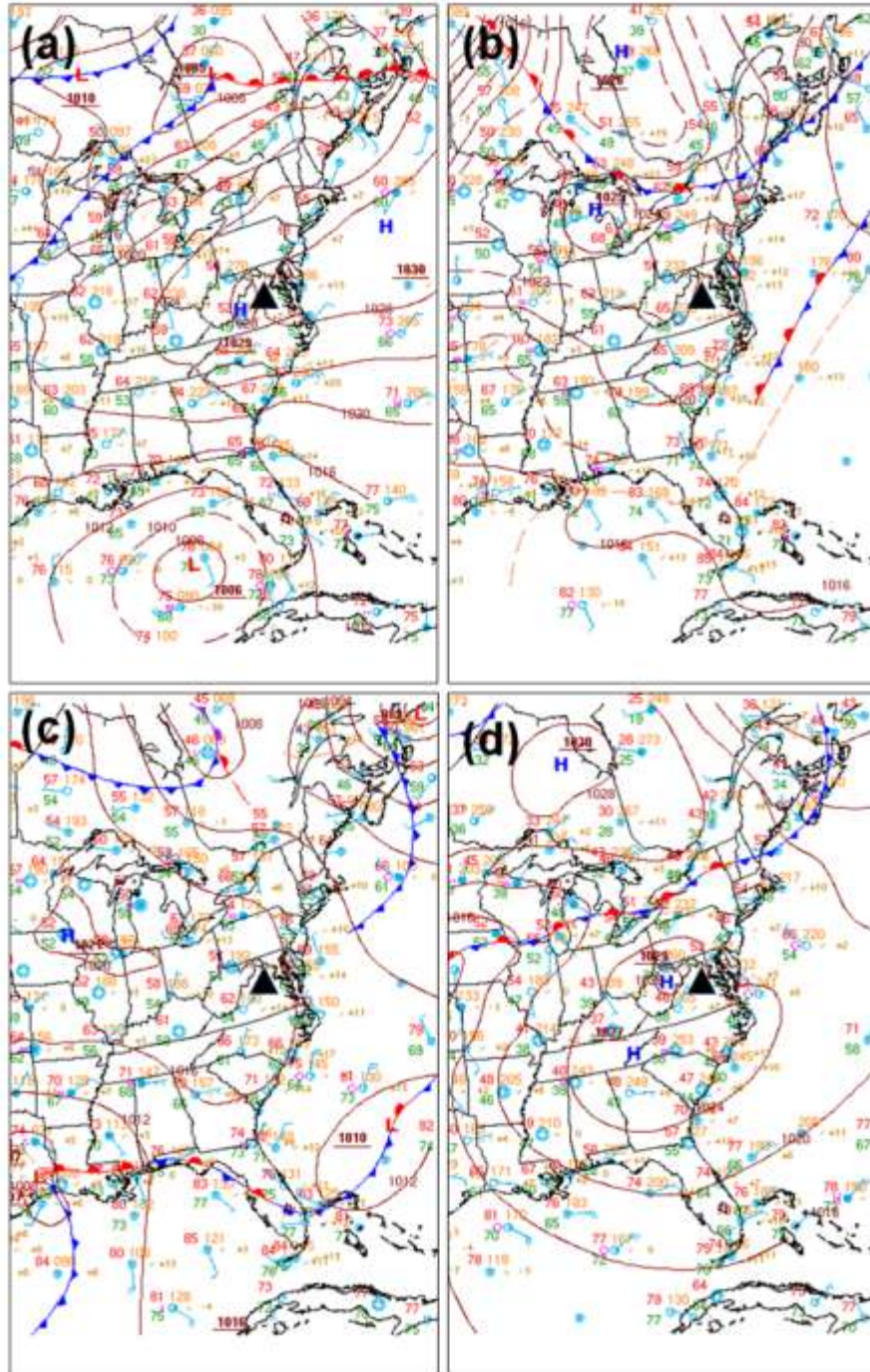
237 Unfortunately, there were no rawinsonde observations from the adjacent Page Valley on any of
238 the four case study days reported here. Lee and De Wekker (2016) used nearby rawinsonde

239 profiles to estimate maximum CBL heights in the Page Valley. Nevertheless, using only daytime
 240 maximum CBL heights, one cannot infer boundary layer transport and mixing processes of trace
 241 gases at a mountaintop site in detail. For instance, to understand the impact of CBL regimes on
 242 the CO mixing ratio during the entire diurnal cycle, it is important to have information on CBL
 243 growth rate, CBL height variability including entrainment processes, and upslope flows. Thus, a
 244 complete picture of daytime evolution of CBL heights over mountaintop, obtained in this study
 245 using continuous lidar measurements, is a pre-requisite to address our research goals.

246 **Table 1:** A summary of the near-surface meteorological conditions on the four case study days.
 247 *CI: Clearness index, T_{max} : Daily maximum temperature, T_{min} : Daily minimum temperature, DTR:*
 248 *Diurnal temperature range calculated by subtracting T_{min} from T_{max} , SHF: Sensible heat flux*
 249

Date in 2009	Diurnal temperature parameters (°C)			CI	Wind direction or observed wind shift	Local standard time	
	T_{max}	T_{min}	DTR			Sunrise	SHF
							crossover
14 Sept	20.66	13.53	7.13	0.77	Westerly (no wind shift) with decreasing wind speed	06:55	07:30
21 May	20.34	13.28	7.06	0.85	Wind shift from NW to SE	06:05	06:25
5 Sept	21.14	16.23	4.91	0.62	Wind shift from NNW to SE	06:50	07:55
21 Oct	18.02	14.21	3.79	0.75	Wind shift from NW to SE	07:30	08:15

250



251

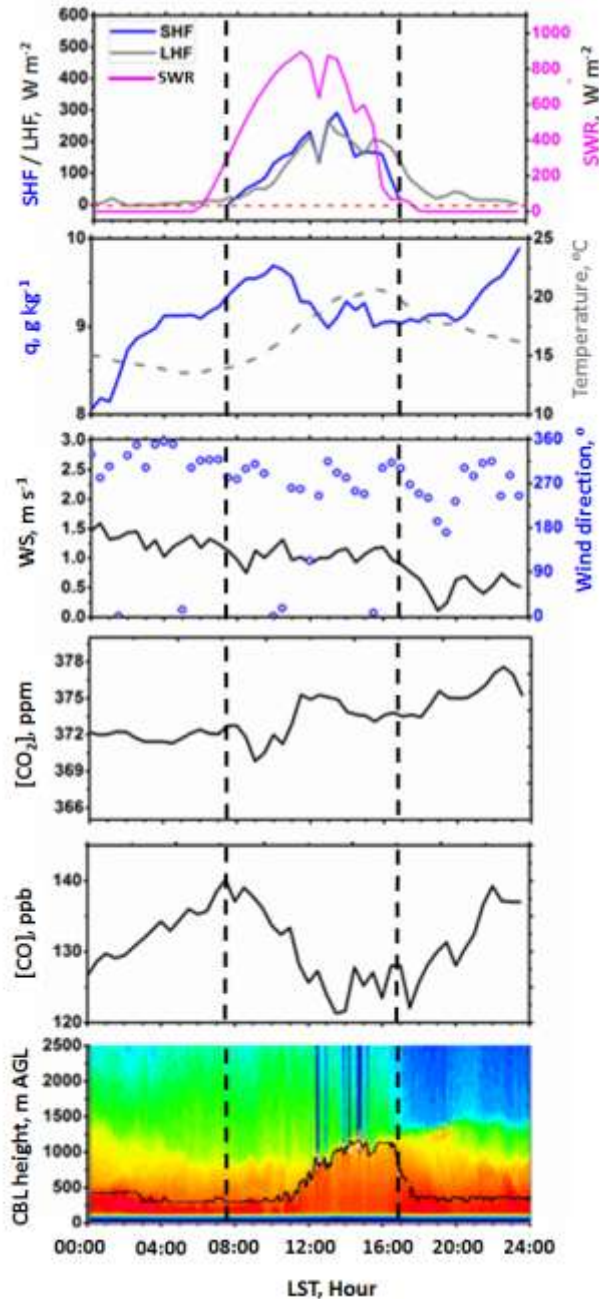
252 **Fig. 2.** Surface synoptic charts at 12:00 UTC (07:00 LST) on 21 May 2009 (a), 5 September
 253 2009 (b), 14 September 2009 (c), and 21 October 2009 illustrating fair weather high-pressure,
 254 anticyclonic synoptic settings on all four days. The location of Pinnacles is denoted by black
 255 triangle. Figures courtesy of <hpc.ncep.noaa.gov>.

256 **5. Results and discussion**

257 **5.1 Case I: Impacts primarily related to boundary layer dilution (14 Sept 2009)**

258 Case I on 14 September 2009 is characterized by clear-sky anticyclonic conditions with weak to
259 moderate westerly winds (Fig. 3). In particular, wind speed observed at 17 m AGL at Pinnacles
260 was rather constant around 1.2 ms^{-1} until 16:00 LST (LST=UTC-5:00); afterwards the wind
261 weakened and remained around 0.5 ms^{-1} while there was a slight backing from northwesterly to
262 southeasterly. Near-surface meteorological measurements reveal that the morning and evening
263 crossover of sensible heat fluxes took place at 07:45 and 17:00 LST, respectively, while sunrise
264 and sunset on this day were around 07:00 and 18:30 LST, respectively. The diurnal temperature
265 range was $9 \text{ }^\circ\text{C}$ while daytime maximum temperature was $22.5 \text{ }^\circ\text{C}$.

266 The time-height cross-section of the lidar measured range-square corrected signals over
267 Pinnacles on this day exhibits a clear-sky CBL regime over the site (Fig. 3). The CBL heights
268 derived using Haar wavelet method on the lidar-derived aerosol backscatter profiles are overlaid
269 (black solid line). Lidar measurements display a “textbook-style” CBL development over the site
270 with a maximum quasi-stationary CBL height about 1250 m AGL. [We have also compared the](#)
271 [lidar-based CBL height estimates with the CBL height measured at the nearest rawinsonde site](#)
272 [\(Dulles airport, IAD\); relevant results and discussion can be found in Appendix A.](#)



273

274 **Fig. 3.** Diurnal cycles of CO_2 , CO , water vapor mixing ratio (q), relative humidity at 17 m AGL
 275 on the tower, heat fluxes and incoming solar radiation, and horizontal wind speed and direction
 276 along with the lidar-measured CBL height at Pinnacles on 14 September 2009. The CBL on this
 277 day reaches a maximum quasi-stationary height of about 1250 m AGL. In the lidar-backscatter
 278 image, cold to warm color denotes lower to higher backscatter intensity. Vertically aligned
 279 dotted lines mark the morning and evening transition period determined using the heat flux
 280 crossover times.

281 We were not able to monitor CBL height <200 m at the site during the measurement period due
282 to incomplete overlap as mentioned before. It can be seen that after 11:00 LST, the CBL height
283 grew at a rate of about 240 m hr^{-1} . Between the morning transition period and the early afternoon
284 hours, the CO mixing ratio of 140 ppb at 07:45 LST decreased by 15 ppb to a quasi-stationary
285 mixing ratio value of 125 ppb between 13:00 and 16:00 LST; this decrease is larger than the total
286 uncertainty (i.e., < 6 ppb [Andrews et al., 2014]) of the CO measurements. This decrease of more
287 than 10 % in CO mixing ratio is consistent with the boundary layer dilution effect. This type of
288 CO diurnal cycle corresponds to the type II scenario (Fig. 1), which is very similar to the
289 observed CO variability on tall tower tops in flat terrain (e.g., Popa et al., 2010). Additionally,
290 measurements of both clearness index and sensible heat flux at the site on this day confirm the
291 presence of a convectively driven boundary layer regime.

292 After 13:00 LST when the CBL top reached its daytime maximum, the CO mixing ratio
293 remained constant around 125 ppb. The CO diurnal cycle at other mountaintop locations often
294 evinces a continuous increase in CO mixing ratios with a daytime maximum due to upslope
295 flows advecting polluted low elevation air from adjacent valleys (e.g., Gao et al, 2005; Henne et
296 al., 2008; Ou-Yang et al., 2014). For the observations presented here, the initial pre-sunrise CO
297 mixing ratio in the atmosphere above the mountaintop is high (~ 140 ppb), and the CO mixing
298 ratio does not increase further after the air mass from the adjacent valley reaches the
299 mountaintop around 09:00 LST. This fact is also evident from the CBL height development,
300 water vapor mixing ratio (q), and CO_2 variability. In contrast, a decrease in the CO mixing ratios
301 was observed from the morning transition period until the early afternoon, which suggests that
302 due to the prevailing deep CBL over the site, the boundary layer dilution effect outweighs the
303 effect due to upslope flows.

304 It should be noted that a steady rise in CO in the very early morning (i.e. between 00:00 and
305 06:00 LST) might correspond to morning local vehicular traffic or campfires near the
306 mountaintop site. One potential source for local vehicular traffic Skyline Drive, a scenic tourist
307 road in the Shenandoah National Park that runs southwest-northeast about 100 m southeast of
308 Pinnacles. However, any vehicular emissions from this road would be advected away from the
309 site because of the northwesterly winds observed between 0000 and 0600 LST on this day.

310 In general, q showed similar variability as the CO mixing ratios, with an increase/decrease in
311 water vapor accompanied by an increase/decrease in CO levels. In particular, the decrease in CO
312 is coincident with the simultaneous decrease in water vapor mixing ratio at the site. Water vapor
313 is also conserved on time scales of CBL mixing, so we examine this tracer along with CO and
314 perform regression analysis between these two parameters. The correlation coefficient (r)
315 between the time series of CO and q for the period between sunrise and sunset was 0.59. Ou-
316 Yang et al. (2014) found similar variability in the seasonal mean diurnal cycles of q and CO for a
317 high-mountain background station in East Asia, and Weiss-Penzais et al. (2006) also found this
318 for Mt. Batchelor Observatory. However, they did not perform any correlation analyses; thus it
319 was not possible to objectively compare their findings with the results presented here. We note
320 that a daytime peak in CO₂ is due to the absence of or only weak CO₂ uptake via photosynthesis
321 during the fall so that the air mass arriving at the site from the adjacent valley due to upslope
322 flows is not CO₂ depleted. This is unlike cases in summer months as discussed, for example, in
323 De Wekker et al. (2009) where a decrease is observed in CO₂ at a mountaintop site in the
324 Colorado Rockies due to photosynthetic CO₂ uptake.

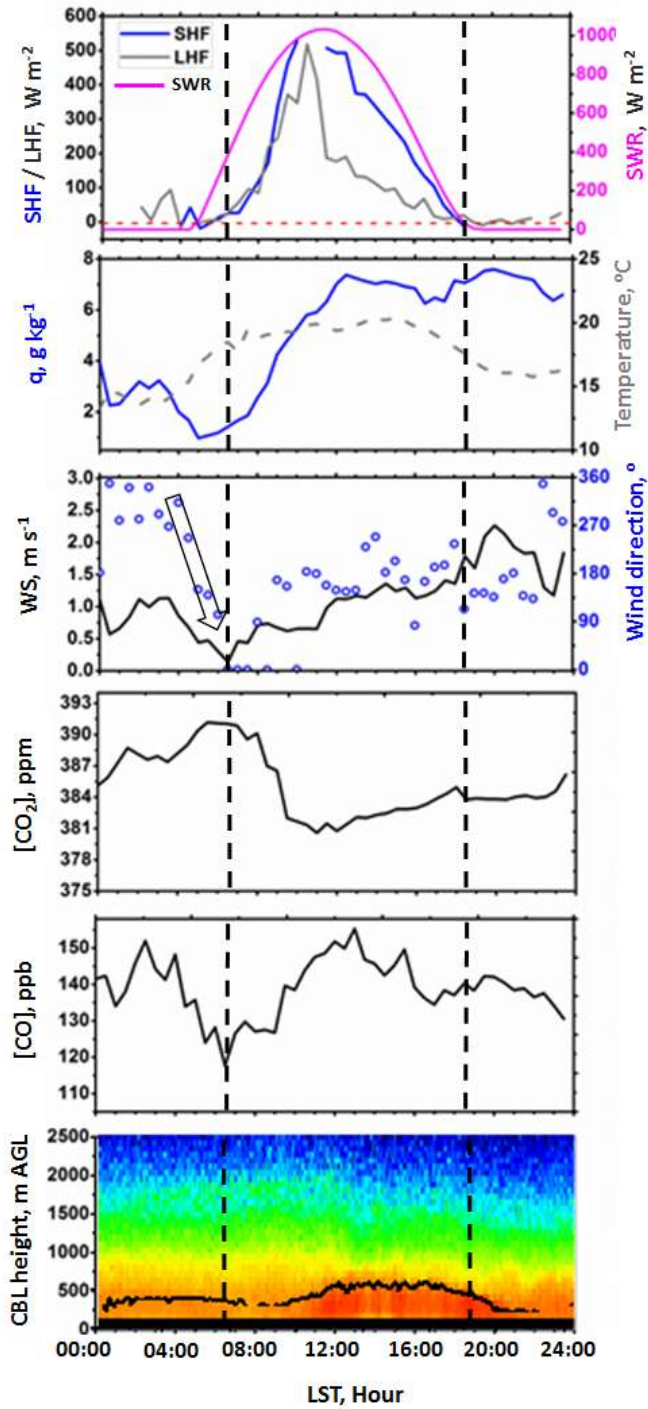
325

326 5.2 Case II: Impacts corresponding to slope flows (21 May 2009)

327 The lidar observations during case II on 21 May 2009 indicate the evolution of a shallow CBL
328 over the site with a maximum CBL height of 550 m AGL around 12:00 LST remaining quasi-
329 stationary for more than 4 hours until 16:30 LST (Fig. 4). The morning CBL growth rate (90
330 m hr⁻¹) was slower than for case I (240 m hr⁻¹). The CBL height at IAD using the 19:00 LST
331 sounding on 21 May was 1306 m MSL, using the approach in Lee and De Wekker (2016); see
332 Appendix A for further details.

333 Starting at 06:30 LST in the morning, both CO mixing ratios and q exhibit an increasing trend
334 until 12:00 LST when the CBL reached its daytime maximum value. This increasing trend
335 illustrates the impact of upslope flow on the CO mixing ratios. The correlation between CO and
336 q was higher ($r = 0.75$) than for case I. The CO mixing ratio increased from an initial value of
337 116 ppb to 155 ppb at 13:00 LST. This large increase in CO mixing ratio may be attributed to
338 transport from local upwind source regions and corresponds to type I scenario (Fig. 1). Also, in
339 contrast to case I, the CO₂ diurnal cycle for this case evinces noticeable impact of upslope flow
340 and associated photosynthetic uptake on the diurnal variability with a more prominent decrease
341 in daytime CO₂ mixing ratios as discussed in previous studies for situations in the growing
342 season (e.g., De Wekker et al., 2009; Lin et al., 2016). Additionally, to help determine local
343 sources of CO, we have also investigated the possible local influences from a nearby road
344 (Skyline drive) on the CO mixing ratio at Pinnacles (see Appendix B for further discussion).

345 The increase indicates that CO mixing ratios in the valley air mass reaching the mountaintop via
346 vertical transport and mixing were higher than at the mountaintop, so boundary layer dilution did
347 not have a significant impact on the mountaintop trace gas mixing ratios until 13:00 LST. Thus,



348

349 **Fig. 4.** Same as Fig. 3 but for measurements on 21 May 2009 illustrating CO variability in the
 350 presence of a shallow CBL (~ 550 m AGL). Horizontal wind shift is marked by the black arrow in
 351 the third panel.

352 we infer that the mountaintop measurements are mainly influenced by valley air during a time
353 period until 12:00 LST when continuous development of the CBL height over the mountaintop
354 was observed based on the lidar measurements. In a very recent study, using the measurements
355 from concurrent DISCOVER-AQ (Deriving Information on Surface Conditions from Column
356 and Vertically Resolved Observations Relevant to Air Quality) and FRAPPE (Front Range Air
357 Pollution and Photochemistry Experiment) campaigns in northern Colorado, Sullivan et al.
358 (2016) also illustrated similar impacts of thermally driven flow throughout the day. Their study,
359 which mainly reported on O₃ concentrations, highlighted the role of slope winds on bringing
360 pollutants from the Colorado Plains toward the foothills of the Rocky Mountains.

361 In the afternoon hours between 13:00 and 17:00 when the CBL height remained quasi-stationary
362 around its daytime maximum value, both CO and q mixing ratios decreased. In particular, the
363 CO mixing ratio decreased by around 20 ppb due to the dilution effect. Thus, on a day with a
364 relatively shallow CBL over the mountaintop, the CO mixing ratio is affected by upslope flows
365 during the growing CBL regime and by the dilution effect when CBL reaches its daytime
366 maximum until the late afternoon. However, in the deep CBL scenario (i.e. case I), the CO at the
367 mountaintop was influenced mainly by the CBL dilution effect.

368 The CO diurnal cycle feature during the morning transition period observed for case II is similar
369 to the CO measurements at the tops of tall towers in flat terrain: vertical transport and mixing of
370 polluted NBL air to the tower top increases the CO mixing ratio until the time when the CBL
371 height reaches the tower height during the late morning or early afternoon hours (e.g., Yi et al.,
372 2000; Pal et al., 2015; Pal and Haeffelin, 2016). However, for tall tower measurements in flat
373 terrain, the tracer mixing ratios remain in their equilibrium level during the quasi-stationary CBL

374 regime whereas for the mountaintop site the CO mixing ratios continue decreasing due to CBL
375 dilution until 17:00 LST.

376 The CO diurnal cycle feature for Case II is unlike the diurnal cycle reported by, e.g., Gao et al.
377 (2005) at Mount Tai in China where they attributed the elevated afternoon mixing ratios of CO to
378 the transport of boundary layer pollution to the summit of the mountain due to daytime upslope
379 flows and the growth of CBL. In that case, the dilution effect was not able to overcome the
380 increase in CO due to upslope flows. Nevertheless, Gao et al. (2005) did not investigate the
381 mountaintop CBL evolution as we have presented here using continuous lidar measurements.

382 Additionally, it should be noted that the CO mixing ratio between 01:00 and 04:00 LST appears
383 to be as large as during the daytime upslope regime on this day, which suggests that during a
384 time period without upslope flows, near peak CO is sampled which most likely can be attributed
385 to the RL CO mixing ratio at the site. Then, between 03:00 and 06:00 LST, i.e. near sunrise but
386 before upslope flow can properly occur, CO begins to decrease. This decrease occurs
387 simultaneously with a wind shift from northwesterly to southeasterly illustrating the impact of
388 local-scale transport processes on the CO mixing ratio at the monitoring site. This suggests air
389 masses being transported downslope by the cold drainage flow at night affecting the CO mixing
390 ratio at the site in the early morning. Water vapor mixing ratio also decreases by 2 g kg^{-1} during
391 the same period (i.e. between 03:00 and 06:00 LST).

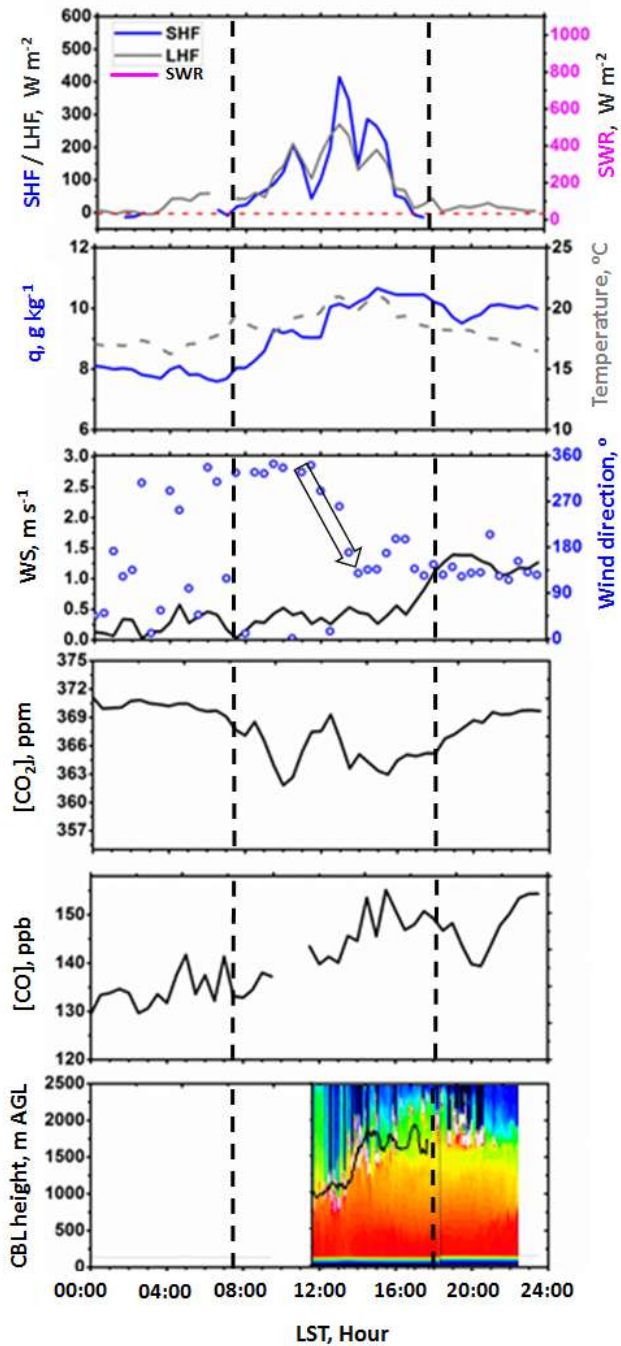
392 **5.3 Case IIIa: Impacts corresponding to horizontal transport (5 September 2009)**

393 Very different meteorological conditions and trace gas variability were observed during case IIIa
394 on 5 September 2009 than during the previous two cases. During this case, a clearly visible
395 daytime horizontal wind shift from northwesterly to southeasterly occurs at the site (Table 1 and

396 Fig. 5). Using 4-years long measurements, recently, Lee et al. (2015) concluded that the
397 horizontal transport of CO outweighs the dilution effect resulting in a daytime increase in the CO
398 mixing ratio due to wind shift. In the present context, CO variability during case IIIa at Pinnacles
399 (i.e. C_{M_Top} mentioned in Fig. 1) corresponds to type I scenario (section 2) where a clearly visible
400 increase in CO mixing ratio is revealed starting around 12:00 LST. The temporal variability of
401 CBL height over the site and its influence on the CO mixing ratios were not investigated in Lee
402 et al. (2015). In addition, Pal et al. (2014) found for a valley location that regular wind shifts due
403 to thermally driven valley flows affect the variability of ultrafine aerosol particles where
404 advection outweighs the contribution of CBL mixing. These two recent studies motivated us to
405 further investigate the impact of wind shifts on the CO mixing ratio on diurnal time scales using
406 concurrent lidar and meteorological measurements at Pinnacles. Consequently, we selected two
407 cases with well-defined diurnal wind shift.

408 Lidar measurements were not available during case IIIa for the period between midnight and
409 noon. However, CBL height measurements during the afternoon reveal the development of a
410 deep CBL over the site. The CBL height shows a daytime maximum of 1500 m AGL around
411 15:00 LST when low level clouds appeared at the site. At this time, the horizontal wind started
412 backing from northwest to southeast. Very low wind speeds ($\sim 0.5 \text{ ms}^{-1}$) were observed during
413 the first half of the day. After 16:00 LST, the wind speed increased from 0.5 to 1.5 ms^{-1} and
414 remained southeasterly until midnight.

415 The observed wind shift at the site around 12:00 LST (northwesterly to southeasterly) is most
416 likely not suggestive of slope flows on this day at the site. For instance, the occurrence of the
417 low-level clouds influenced both the sensible and latent heat fluxes as well as the near-surface
418 temperature measurements. In particular, the diurnal cycle of sensible heat flux was disrupted on



419

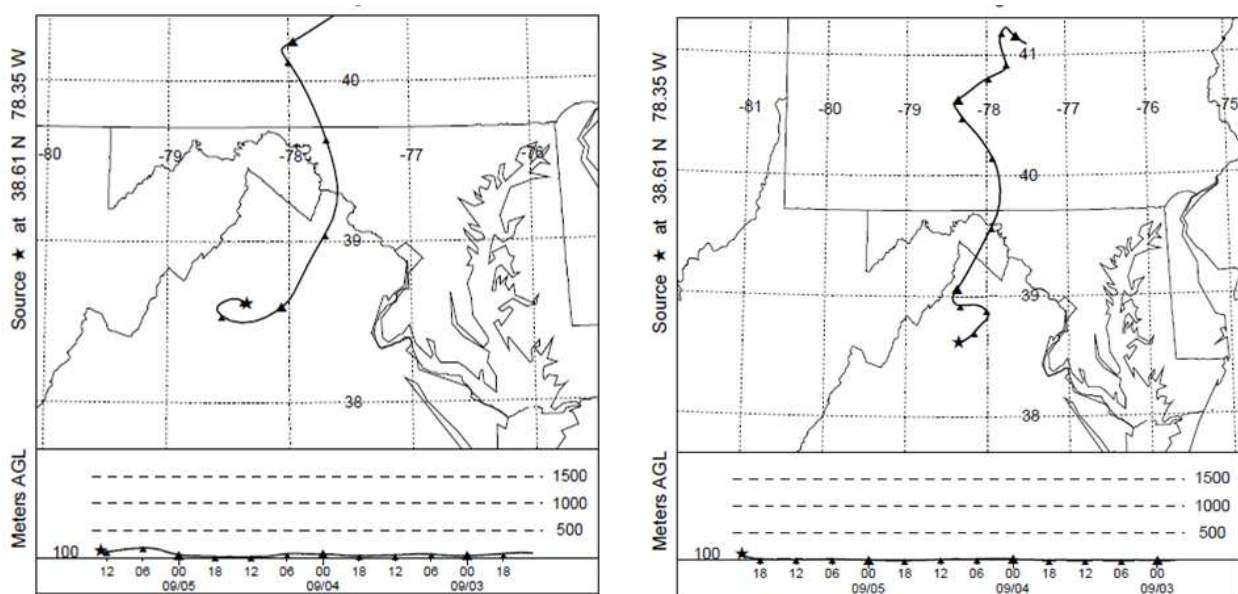
420 **Fig. 5.** Same as Fig. 3 but for measurements on 5 September 2009 for case IIIa revealing the
 421 influence of daytime horizontal wind shift from (northwesterly to southeasterly) on the CO
 422 variability. The development of a deep CBL (1500 m AGL) on this day over the site is also
 423 visible. Horizontal wind shift is marked by the black arrow in the third panel.

424 this day, contrary to the two previous cases. The daytime maximum and nighttime minimum
425 temperatures were 21 °C and 16 °C, respectively, and showed no prominent diurnal cycle that
426 had been observed in the other cases. Additionally, synoptic surface analyses also indicated
427 similar wind shift at other sites over the adjacent plains (not shown).

428 During case IIIa, the CO mixing ratio increased by 10 ppb between 08:00 and 11:00 LST
429 whereas during the afternoon between 12:00 and 15:00 LST, a relatively larger increase (15 ppb)
430 in CO was observed, and CO mixing ratios peaked at 150 ppb. The q variability was similar to
431 the CO variability with a maximum q of 11 g kg⁻¹ at 16:00 LST, remaining high until midnight.
432 The correlation between CO and q variability was higher during this case study than during the
433 two other cases, with r of 0.82.

434 This case appears to completely conflict the mechanism described in Case I that also had a deep
435 CBL over the site. Specifically, we did not observe dominant signatures of boundary layer
436 dilution effect on CO diurnal cycle exhibiting daytime decrease during case IIIa. We investigated
437 the role of the shift in the horizontal wind (northwesterly to southeasterly) to the increase in CO
438 mixing ratio starting at 10:00 LST. To this end, we performed a trajectory analysis of case IIIa
439 using the Hybrid Single Particle Lagrangian Integrated Trajectory (HYSPLIT) model (Draxler
440 and Hess, 2004), which we initialized using 12 km wind fields from the North American Model
441 (NAM) as displayed in Fig. 6. We ran HYSPLIT backward 72 hr using a starting height of 100 m
442 AGL following previous studies in the region (i.e., Lee et al. 2012; Lee et al. 2015). We
443 performed two runs: one for the morning when northwesterly winds were observed at Pinnacles,
444 and another for the afternoon when southeasterly flows were present. Both runs yield the
445 differences in wind direction early on in the backward trajectory analysis and the trajectory goes
446 over a very different area. However, both runs suggest the Northeast is a source region here.

447 Similar findings on the impact of horizontal transport on CO measurements at Pinnacles were
 448 previously reported by Lee et al. (2012). These results suggest that the CO and q variability were
 449 mainly governed by the transport of a different air mass associated with the horizontal wind shift.
 450 In particular, along with the primary maximum in the CO mixing ratio in the late afternoon (~
 451 150 ppb around 15:00 LST), several secondary peaks were also present. Therefore, it is likely
 452 that the boundary layer dilution effect during the late afternoon did not have a clear impact on
 453 the trace gas variability at the site for case IIIa as was evident for case I, although in both cases a
 454 deep boundary layer (1200 m AGL) prevailed.



455
 456 **Fig. 6.** 72 Hour backward trajectory based on NOAA HYSPLIT model using NAM (12 km
 457 horizontal resolution) meteorological data, initialized 100 m AGL for 13:00 UTC (08:00 LST, 5
 458 Sep 2009), (left) and 21:00 UTC (16:00 LST), (right). Model vertical velocity was used for
 459 vertical motion calculations for both scenarios. Height of trajectory AGL is shown in the bottom
 460 portion of the figure. Source of the images <http://ready.arl.noaa.gov/HYSPLIT.php>.

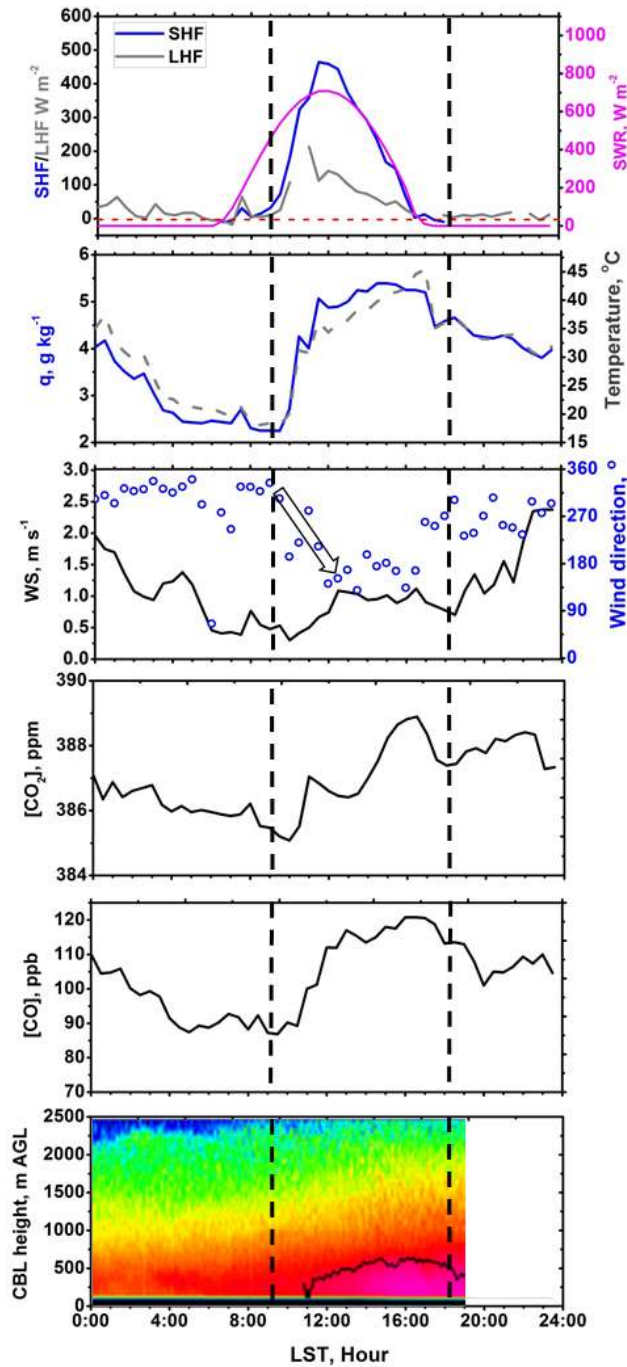
461
 462
 463

464 **5.4 Case IIIb: Impacts corresponding to horizontal transport (21 October 2009)**

465 To further illustrate the role of horizontal wind shift on CO mixing ratios, we considered another
466 case (i.e., case IIIb, 21 October 2009). During case IIIb, a similar wind direction shift was
467 observed at the site but occurred during the morning transition period around 10:00 LST (Fig. 7).
468 Case IIIb was characterized by cloud free conditions with a clear diurnal cycle in the incoming
469 solar radiation, sensible heat flux, and other meteorological variables at the site (Table 1).
470 However, the CBL was shallower than in previous case (case IIIa) with a daytime maximum
471 CBL height of ~ 500 m AGL.

472 The prevailing northwesterly wind started backing at 10:00 LST and became southeasterly at
473 around 12:00 LST. Between 09:00 and 17:00 LST, CO mixing ratios steadily increased from an
474 average value of around 90 ppb to a maximum value of around 120 ppb; thus corresponds to type
475 I scenario (Fig. 1). The increase in CO mixing ratio of more than 30 ppb is larger than the total
476 uncertainty (i.e., < 6 ppb) of the instrument. The water vapor mixing ratio increased in a very
477 similar way as CO from its early morning value of 2.5 g kg⁻¹ to a quasi-steady afternoon value of
478 5.5 g kg⁻¹. A correlation coefficient between CO and q of 0.91 confirms their similar (or almost
479 identical) temporal variability between sunrise and sunset on this day. After 17:00 LST when the
480 horizontal wind became westerly, both CO and water vapor mixing ratios started to decrease due
481 to downslope flows transporting cleaner FA air masses to the site.

482 One general conclusion from the above results is that, due to a shift in the wind direction (from
483 northwesterly to southeasterly), horizontal advection of a different air mass increases the CO
484 mixing ratio at the site. However, increases in CO mixing ratios in both cases appear to be
485 similar but not identical. In particular, (1) two different CO increases were observed: 20 ppb and

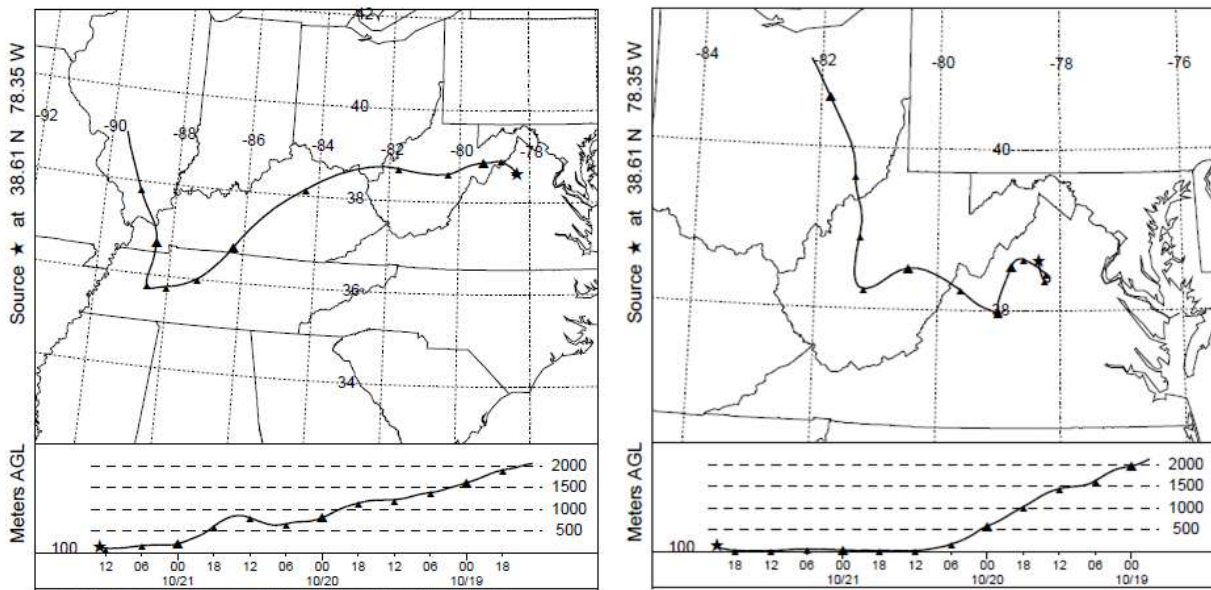


486

487 **Fig. 7:** Same as Fig. 3 but for measurements on 21 October 2009 (case IIIb) illustrating the
 488 impacts of both wind directions shift during the morning transition period and a shallow CBL
 489 (600 m AGL) over the site during the afternoon hours. The initial CO mixing ratio was very low
 490 (90 ppb). Horizontal wind shift is marked by the black arrow on the third panel.

491 35 ppb for case IIIa and case IIIb, respectively; (2) the initial CO mixing ratios (i.e. CO mixing
492 ratio in the NBL at the site) for case IIIa and case IIIb were 130 and 85 ppb, respectively, so
493 more polluted air masses were present during case IIIa than during case IIIb, and (3) lidar
494 measurements confirmed a higher daytime maximum CBL height during case IIIa (1500 m
495 AGL) compared to case IIIb (500 m AGL). Although for both cases the CO mixing ratio
496 variability was substantially influenced by the air mass transported to the site, it appears that the
497 boundary layer dilution effect had more impact on CO mixing ratio during case IIIa than during
498 case IIIb. Thus, a larger increase and more accumulation in CO (35 ppb) were observed for case
499 IIIb than for case IIIa. These results clearly underscore the importance of continuous monitoring
500 of CBL height variability at a mountaintop site like Pinnacles.

501 [Additionally, we have performed HYSPLIT analyses for case IIIb \(21 Oct 2009\) which showed](#)
502 [clear evidence that different air mass source regions influenced the site during the daytime. 72](#)
503 [hour backward trajectories initialized at 0800 LST show descending trajectories that originated](#)
504 [over the Midwest. Backward trajectories initialized at 1600 LST had shorter flow paths and had](#)
505 [more contact with surface emissions over central Virginia, thereby helping to explain the marked](#)
506 [increase in CO mixing ratios observed at the site during the afternoon.](#)



507

508 *Fig. 8. Same as Fig. 6 but for 72 Hour backward trajectory, initialized at 100 m AGL for 13:00*

509 *UTC (08:00 LST, 21 Oct 2009), (left) and 21:00 UTC (16:00 LST), (right). Source of the images*

510 *<http://ready.arl.noaa.gov/HYSPLIT.php>.*

511 6. Generalization of the case studies

512 Using lidar-derived CBL height variability over a mountaintop site, we demonstrated for the first

513 time the relation between CBL height and CO mixing ratio for a typical well-characterized

514 situation at a low mountaintop site (Pinnacles). This investigation helped us provide detailed

515 information on diurnal cycles of CO mixing ratios, in particular, contrasting CO diurnal cycles:

516 daytime decrease (case I with daytime maximum CBL height of around 1200 m AGL) versus

517 daytime increase (case II with daytime maximum CBL height of around 500 m AGL).

518 Additionally, two cases (cases IIIa and IIIb) with diurnal wind shift illustrate the role of transport

519 of a different air mass to the site on the elevated afternoon levels of CO and water vapor mixing

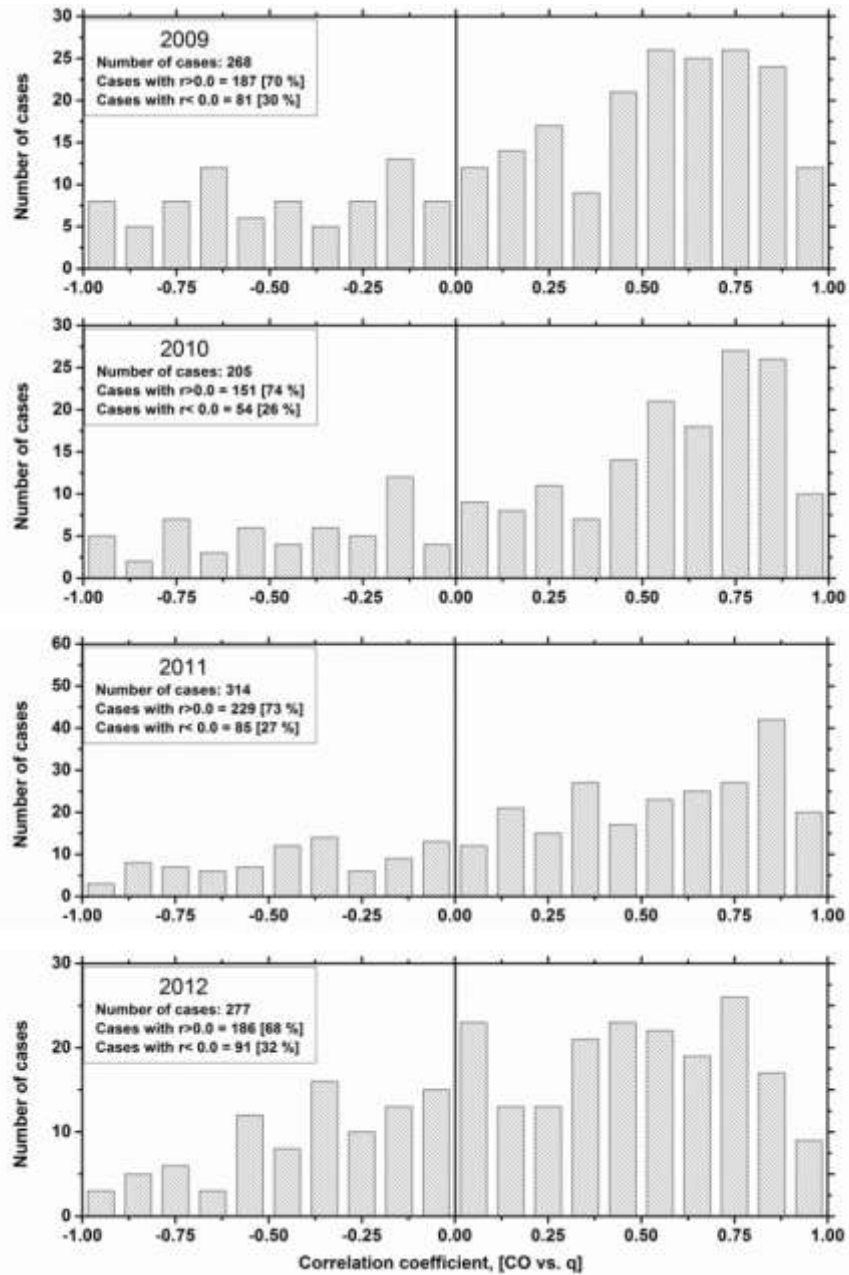
520 ratios as was reported by Lee et al. (2015) although their work did not provide detailed
521 information on the CBL height evolution at the site.

522 In recent studies, researchers have started examining the implications of using nocturnal versus
523 daytime mountaintop measurements of GHGs and trace gases within model simulations (e.g. Lin
524 et al., 2016). Additionally, very recently, Bamberger et al. (2017) investigated the application of
525 mountaintop measurements to find regional representativeness GHG mixing ratios. Our findings
526 further illustrate CO mixing processes in complex terrain, in particular over a site significantly
527 perturbed via local scale flows. Two key aspects of the results presented in Section 5 are
528 generalized here by evaluating four-year (2009-2012) long measurements of CO and
529 meteorological conditions at Pinnacles: (1) correlation between daytime CO and water vapor
530 mixing ratio evolution, and (2) general pattern of diurnal contrasts in CO mixing ratios.

531 **6.1 Correlation between daytime CO and water vapor mixing ratio evolution**

532 A linear regression analysis was carried out between CO and water vapor mixing ratio variability
533 from sunrise to sunset on each day of the four-year period that we performed for the case studies
534 presented in Section 5. Frequency distributions of the correlation coefficients (r) for different
535 years are shown in Fig. 9. As discussed in Section 5, positive (negative) correlation coefficient
536 implies that both CO and q vary similarly (differently). Numbers of cases vary from one year to
537 the other; however, at least 70 % of the days in a year are covered (except in 2010 where number
538 of days is 205).

539 Nevertheless, it can be concluded that 70 % (30 %) of the times in a year, CO and q shows a
540 positive (negative) correlation coefficient illustrating the fact that like q , CO could be considered



541

542 **Fig. 9.** Distribution of r based on regression analyses between daily time series of CO and q

543 between morning transition period to late afternoon on different days between 2009 and 2012.

544 Number of cases in different years, two different r distributions with number of days and

545 percentages with respect to the total number of days when observations were available are

546 reported in each panel. Vertically-aligned solid grey line marks $r = 0$ showing no correlation

547 between CO and q .

548 a good tracer for studying boundary layer mixing processes including the impact of upslope
549 flows in the mountainous regions. For instance, in 2009, positive (negative) r was found on 187
550 (81) days among 268 days. In section 5, it was found that available lidar-derived CBL height
551 variability helped understanding the boundary layer regimes at the site for those cases. However,
552 we do not have continuous lidar measurements for the four-year period (2009-2012). In future
553 studies, we will therefore use model simulations of CBL height diurnal cycles and available
554 meteorological measurements to illustrate possible mechanisms governing the nature of
555 correlation coefficients on different days and seasons at the site.

556 **6.2. General pattern of diurnal contrasts in CO mixing ratios**

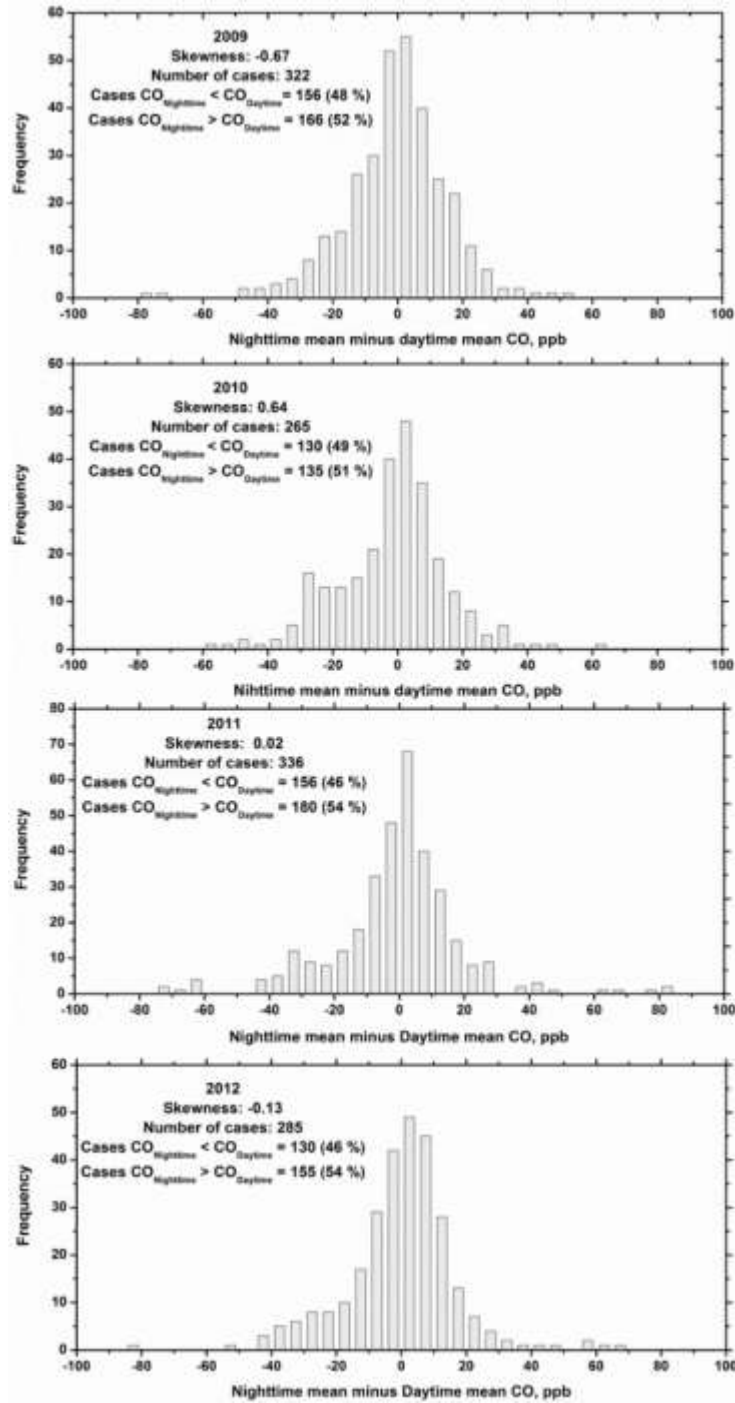
557 In this study as well as in a number of past studies, it was found that due to upslope flow
558 contribution, CO mixing ratio at the mountaintop sites increases after morning transition and
559 yields a daytime maximum peak (case II). However, within the case studies presented here, we
560 demonstrated that for some situations the boundary layer dilution effect outweighs the upslope
561 flow contribution in governing CO diurnal cycle and yields a daytime minimum (case I). Thus,
562 using the four-year long measurements at Pinnacles we demonstrate how frequent the two
563 different types of CO diurnal cycles (i.e. [type I and type II scenarios in Fig. 1](#)) occur at the site
564 using daytime versus nighttime CO differences on different days. We believe these results would
565 provide important information on the interplay between the nocturnal CO mixing ratios at the
566 mountaintop versus the upslope flow contribution and boundary layer dilution.

567 First of all, daily mean nocturnal (daytime) CO mixing ratio is determined by averaging CO
568 variability observed between 00:00 and 04:00 LST (12:00 and 16:00 LST). [We refer to the](#)
569 [difference between nighttime and daytime CO as the “CO contrast” on diurnal time scale.](#) The

570 daily CO contrast is obtained by subtracting the daytime mean from nighttime mean CO mixing
571 ratio. As explained in section 5, a positive CO contrast implies a decrease in CO mixing ratios
572 during the day, most likely explaining the impact of boundary layer dilution while a negative CO
573 contrast implies an increase in CO mixing ratios during the day, most likely explaining the
574 impact of upslope flows bringing more polluted adjacent valley air mass or via transport of a
575 different air mass to the site.

576 Results obtained for the CO contrasts on different days between 2009 and 2012 are summarized
577 in Fig. 10. For instance, in 2009, the number of days or cases showing a daytime increase (156
578 days among 322) is very similar to the number of cases showing a daytime decrease (166 days
579 among 322) at the site illustrating comparable situations for both the impacts of upslope flows or
580 transport processes and boundary layer dilution effect. It can also be seen that in other years
581 these contributions remain comparable (i.e. ~ 50 %) suggesting the importance of continuously
582 monitoring both meteorological conditions and CBL heights over the low mountaintop sites like
583 Pinnacles. These results will help demonstrate the implications of assimilating nighttime versus
584 daytime measurements within numerical models for low mountaintops. In future studies, using
585 long-term measurements of CO contrasts and model-simulations of CBL height and
586 meteorological conditions, we will investigate in detail the diverse nature of the reported CO
587 contrasts.

588



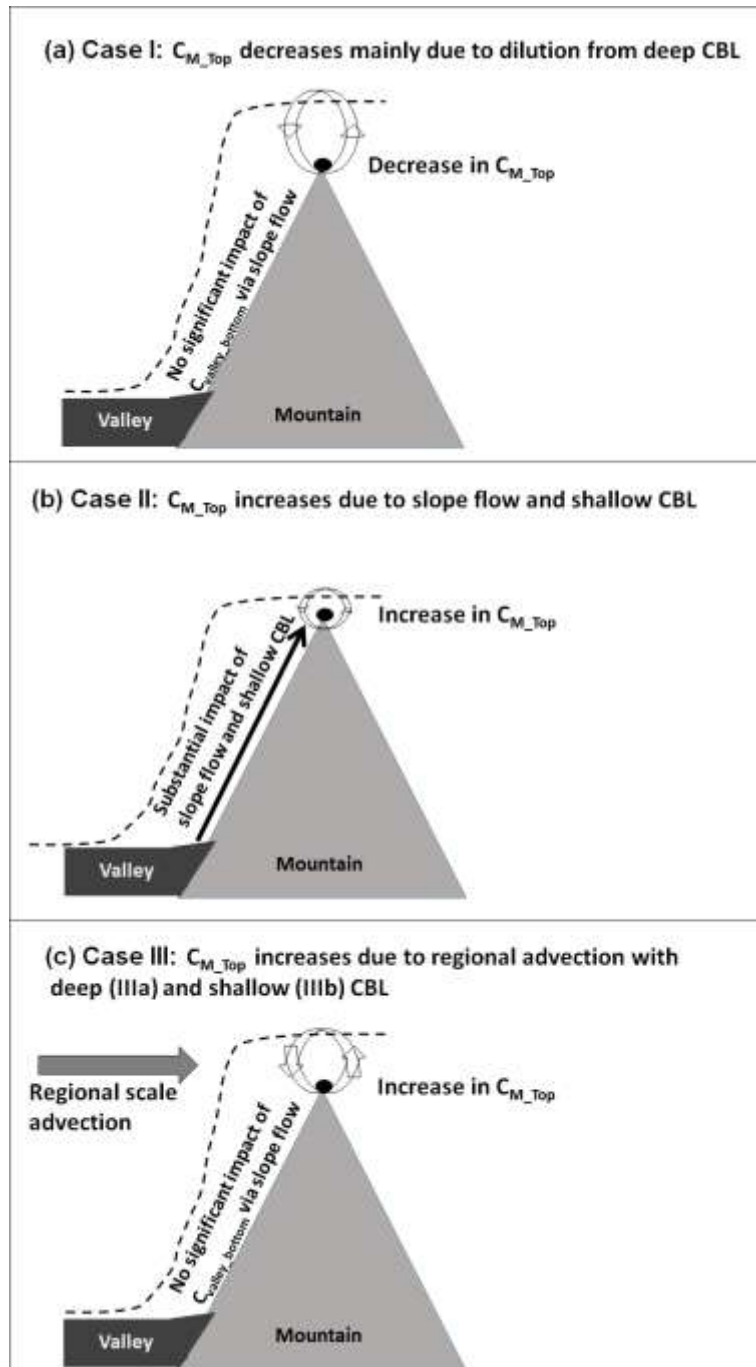
589

590 **Fig. 10.** CO contrasts calculated by subtracting daytime mean CO mixing ratio from nighttime
 591 mean CO mixing ratio on different days for the period between 2009 and 2012. Numbers of
 592 cases in two different regimes of CO variability with their occurrences are also reported in each
 593 panel.

594 7. Summary, conclusions and outlook

595 In the present study, we used selected case studies to investigate the impact of CBL dynamics on
596 the diurnal variability of CO mixing ratio at a low mountaintop site. We hypothesized that CO
597 diurnal cycle at the mountaintop site is affected by the combined impact of meteorological
598 condition, slope flows, boundary layer depth and associated growth rate, and regional scale
599 advection. We also considered two well-defined clearly two scenarios in the CO diurnal cycle:
600 Type I scenario for increasing CO, and type II scenario for decreasing CO. Using three different
601 cases, we find that the CO diurnal cycle during case I (decreasing CO), case II (increasing CO),
602 and case III (increasing CO) is significantly affected by deep CBL mixing, upslope flow, and
603 regional scale advection, respectively. A summary of the findings for the three cases is illustrated
604 in Fig. 11 which clearly outlines the fact that one needs to untangle the influences of competing
605 physical processes affecting mountaintop CO measurements to understand and simulate
606 mountaintop tracer measurements. Investigating the three cases using the available observations
607 facilitated a better understanding of the impacts of CBL dynamics on the CO diurnal cycle over
608 the mountaintop site Pinnacles. In particular, we introduced a conceptual framework for the
609 pollutant mixing processes in the mountain-valley atmosphere using the results based on case
610 studies (Fig. 11).

611 For the first time, continuous and simultaneous lidar and CO measurements during the entire
612 diurnal cycle were performed over a low mountaintop site. We found the following two main
613 results: (1) for a case with initial CO mixing ratios of ~ 120 ppb in the morning and with a
614 shallow afternoon CBL ~ 550 m AGL, a daytime increase in CO is observed, illustrating the



615

616 **Fig. 11:** Summary of the findings for three cases presented in section 5. A decrease in CO mixing
 617 ratio (referred as C_{M_Top} in schematic) during case I occurs mainly due to deep CBL (a), an
 618 increase in CO during case II occurs due to slope flows marked with the black solid arrow (b),
 619 and an increase in CO during case IIIa and IIIb occur due to regional scale advection as marked
 620 by the horizontally aligned arrow (c). The curved dashed line and thick circular arrows in all
 621 panels illustrate the growing CBL and entrainment mixing at the CBL top, respectively.

622 impact of upslope flow contribution (scenario I in schematic presented in Fig. 1). In another case,
623 with initial CO of ~ 140 ppb and daytime CBL height of 1200 m AGL, the CBL dilution
624 outweighs the upslope contribution, illustrating the impact of deep CBL mixing over the site
625 (scenario II); (2) Comparison of two cases with and without horizontal wind shift, (case III and I,
626 respectively), confirm the potentially dominant role of a wind shift and illustrates how elevated
627 afternoon levels of CO and water vapor mixing ratios can be due to the transport of a different air
628 mass to the site with no significant impact of the CBL dilution effect.

629 For typical meteorological conditions and CBL (e.g. case I with daytime maximum CBL height
630 of 1250 m AGL), mountaintop CO measurements have characteristics of monitoring sites in flat
631 terrain. On the other hand, for shallow CBL regime (case II with daytime maximum CBL height
632 of 550 m AGL) over mountaintop, there are some similarities but also some differences with tall
633 tower measurements. For instance, for tall tower measurements, CO mixing ratios remain in their
634 equilibrium level during the quasi-stationary CBL regime in the early afternoon hours whereas
635 for the mountaintop measurements the CO mixing ratios continue decreasing due to CBL
636 dilution until very late in the day (17:00 LST in our case). This knowledge could be used in
637 applications requiring regionally representative CO mixing ratio values.

638 Results presented in this work can help define fruitful criteria for emission regulations and create
639 better quantitative information for the regulatory community. The wind shifts result in different
640 upwind emission sources being sampled and can help estimate emissions and reduce flux
641 estimate uncertainties over upwind areas.

642 This study suggests that the interpretation of observed CO diurnal cycles near the surface at
643 mountaintop sites requires knowledge of the relationship between local CBL dynamics involving

644 mountaintop and adjacent valleys and associated meteorological characteristics given the
645 difficulty in resolving the terrain and flows in complex terrain. For instance, regression analysis
646 between CO and q time series between sunrise and sunset showed positive r in all the cases. We
647 carried out an investigation of the long-term data sets of both quantities and found that CO and q
648 evinces a positive correlation coefficient on $\sim 70\%$ of the days in any given year. Additionally,
649 since the present study is based on four different cases with particular behavior in CO variability,
650 one may wonder about the frequency of these two contrasting CO diurnal cycle features (daytime
651 increase versus decrease in CO mixing ratios). Based on the investigation on the differences
652 between the daily NBL CO and the daytime mean CO mixing ratios, we found that nearly 50 %
653 of the days in any given year, mountaintop CO diurnal cycle exhibit a daytime increase and the
654 rest of the days in a year exhibit a daytime decrease.

655 One of the limitations of the results presented here is that the aerosol lidar measurements at
656 Pinnacles only account for daytime evolution of the CBL heights over the site as the full overlap
657 of the lidar transceiver is attained at a height of 200 m. Thus, it was not possible to determine
658 NBL height and consequently explore further the nighttime CO variability. Additionally, long-
659 term continuous lidar measurements were not available at the site. Although this study is based
660 on four selected cases illustrating concurrent observations of lidar-derived CBL heights, CO
661 mixing ratio and meteorological measurements, it nonetheless underscores the important role of
662 the impact of CBL height variability and slope winds on the CO mixing ratio at the mountaintop.

663 In future work, we will continue to broaden and generalize the results from the selected case
664 studies by evaluating long-term measurements of CO available at the site in combination with
665 estimates of nearby rawinsonde measurements of CBL heights. Such a study will be able to
666 reveal the impact of regional scale CBL height relative to the mountaintop on CO variability.

667 Nevertheless, the present study provided detailed insights into the important factors and physical
668 processes occurring in a mountain-valley atmosphere system. Such insights are helpful for
669 addressing an important and compelling issue: can mountaintop measurements provide high
670 quality data and spatial representativeness similar to a tall tower in a flat terrain? Within future
671 studies, we will use numerical simulations (e.g., the Weather Research and Forecasting (WRF)
672 model) to further examine the role of upslope flows on the mountaintop CO and CO₂ mixing
673 ratios. Finally, while the present study has focused solely on the dynamical processes affecting
674 the mountaintop CO mixing ratios, additional studies are needed to help quantify the potential
675 role of atmospheric chemistry processes on the CO diurnal pattern at low mountaintops.

676 **Acknowledgement**

677 We thank employees from Shenandoah National Park and students at the University of Virginia
678 Department of Environmental Sciences for helping maintain data collection at Pinnacles. We
679 also would like to thank A. Andrews, J. Kofler and J. Williams from NOAA/ESRL for technical
680 and scientific discussions on the CO and CO₂ data. This research and the maintenance of
681 Pinnacles were funded by a MOU between NOAA/ESRL GMD, UVA, by NOAA award
682 NA13OAR4310065, and by NSF Grant ATM-1151445. The synoptic maps used for this research
683 were obtained from NOAA (<ftp://ftp.hpc.ncep.noaa.gov/sfc/>). We also would like to thank
684 two anonymous reviewers for their objective assessments and very useful suggestions, which
685 helped, improve the scientific and technical contents of the article.

686

687 **Appendix A: CBL height derived using lidar at Pinnacles versus rawinsonde at IAD**

688 There were no rawinsonde measurements from the adjacent Page Valley on any of the four case
689 studies presented here. However, we took an advantage of the nearby rawinsonde measurements

690 taken at 19:00 LST (00:00 UTC) at Dulles airport (IAD), located approximately 90 km northeast
691 of Pinnacles near Washington, DC.

692 The CBL height at Dulles airport may be ill-defined around 19:00 LST, considering that NBL
693 evolution has started around that time. Lee and De Wekker (2016) explained that near-surface
694 stability is an important issue that needs to be considered in order to correctly estimate the
695 afternoon CBL height using measurements at 19:00 LST. In their study, they hypothesized that
696 the residual layer height observed at 19:00 LST is equivalent to the daytime maximum afternoon
697 CBL height (Stull, 1988). Therefore, based on an objective method, they excluded the first few
698 hundred meters of stable boundary layer measurements to derive the CBL height from the 19:00
699 LST rawinsonde measurements. We used their methodology to derive afternoon CBL height in
700 this study. The CBL height based on IAD rawinsonde measurements can differ from the CBL
701 height over Pinnacles because of the horizontal distance between the two sites (~ 100 km) and to
702 the two different sampling times of these measurements. Lee and De Wekker (2016) showed
703 typical differences of the CBL height between Dulles and the Page Valley of 200-400 m (higher
704 over the Page Valley than at IAD).

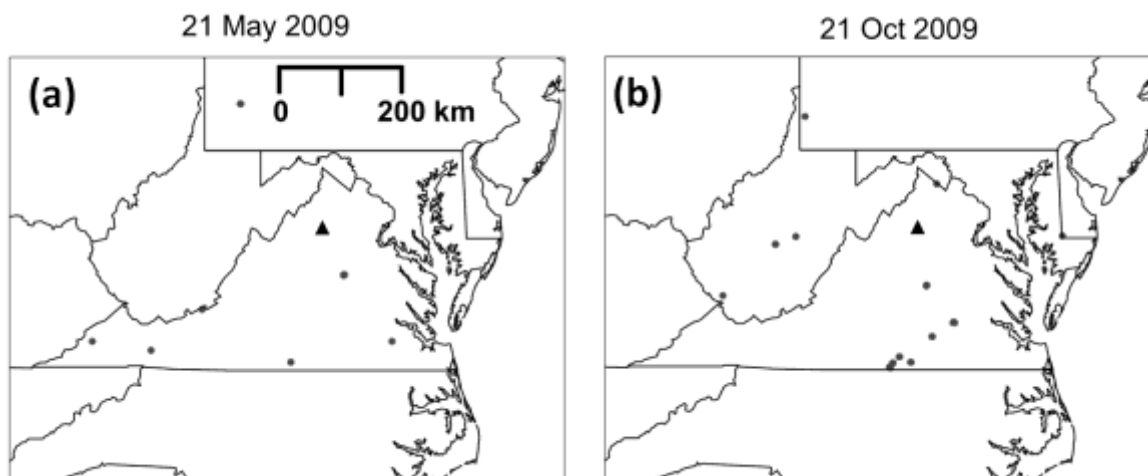
705 For case I (14 Sep 2009) lidar measured daytime maximum CBL height was found to be ~ 1250
706 m AGL over Pinnacles (i.e. ~ 2250 m MSL), whereas CBL height from rawinsonde
707 measurements at 19:00 LST, computed using the bulk Richardson number approach (Lee and De
708 Wekker, 2016), was 1625 m MSL. For Case II (21 May 2009), the CBL height at IAD (1306 M
709 MSL) was also lower than lidar-derived CBL height (~ 1600 m MSL) at Pinnacles. These
710 differences in CBL height between the mountaintop and at IAD are consistent with findings by
711 Lee and De Wekker (2016) who observed spatial heterogeneity in the CBL heights and discussed

712 in detail the different factors responsible for these differences, including the distance between the
713 two measurement sites and the effects of underlying land surface forcing.

714 **Appendix B: Possible impact of local sources of CO at Pinnacles**

715 One notable local source for CO measurements at Pinnacles is Skyline Drive, a scenic tourist
716 road in the Shenandoah National Park that runs southwest-northeast about 100 m southeast of the
717 monitoring site. As Skyline Drive is directly upwind of Pinnacles throughout much of the
718 daytime on 21 May and 21 Oct, one may expect these local emissions to affect the mountaintop
719 trace gas measurements. However, previous studies from the site have suggested that vehicular
720 emissions from Skyline Drive are unlikely to have a significant effect on the mountaintop trace
721 gas measurements from Pinnacles (i.e., Lee et al. 2012, 2015), as well as other nearby
722 mountaintop monitoring sites, i.e. Big Meadows (e.g., Poulida et al., 1991; Cooper and Moody,
723 2000). For example, Lee et al. (2012) found that, despite weekends having 2-3 times the volume
724 of traffic on weekdays, there were no statistically significant differences in trace gas mixing
725 ratios by Skyline Drive. Additional analyses by Lee et al. (2015) confirmed this finding as well.
726 They found that, even though vehicular emissions are typically higher during the summer and
727 fall tourist seasons, CO increases occurred only several hours after the traffic maximum along
728 Skyline Drive.

729 To investigate transport from more regional resources, e.g. upwind fires, we used Moderate
730 Resolution Imaging Spectroradiometer (MODIS) (e.g. Justice et al. 2002) to determine the
731 presence of fires in the region around Pinnacles on days when there is a marked CO increase
732 (e.g., 21 May 2009 and 21 Oct 2009). Analyses of MODIS data for 21 May (Fig. A1a) and for 21
733 Oct (Fig. A1b) indicate the presence of fires upwind of Pinnacles that could have contributed to
734 the daytime CO increase.



735

736 Fig A1: Locations of fires (grey dots) identified in MODIS relative to Pinnacles (black triangle)
 737 on 21 May 2009 (a) and 21 Oct 2009 (b).

738 **References**

739 Andrews, A.E., Kofler, J.D., Trudeau, M.E., Williams, J.C., Neff, D.H., Masarie, K.A., Chao,
 740 D.Y., Kitzis, D.R., Novelli, P.C., Zhao, C.L., Dlugokencky, E.J., Lang, P.M., Crotwell, M.J.,
 741 Fischer, M.L., Parker, M.J., Lee, J.T., Baumann, D.D., Desai, A.R., Stanier, C.O., De Wekker,
 742 S.F.J., Wolfe, D.E., Munger, J.W., and Tans, P.P., 2014. CO₂, CO, and CH₄ measurements from
 743 tall towers in the NOAA Earth System Research Laboratory's Global Greenhouse Gas Reference
 744 Network: instrumentation, uncertainty analysis, and recommendations for future high-accuracy
 745 greenhouse gas monitoring efforts. *Atmospheric Measurement Techniques* 7, 647-687.

746 Atlas, E. L., and Ridley, B. A., 1996. The Mauna Loa Observatory photochemistry experiment:
 747 introduction. *J. Geophys. Res.* 101(D9), 14531-14541.

748 Behrendt, A., Wagner, G., Petrova, A., Schiler, M., Pal, S., Schaberl, T., and Wulfmeyer, V.,
 749 2005. Modular lidar systems for high-resolution 4-dimensional measurements of water vapor,
 750 temperature, and aerosols, in: *Lidar Remote Sensing for Industry and Environment Monitoring*

751 V, Proceedings of SPIE, edited by: Singh, U. N. and Kohei Mizutani, 5653, Honolulu, Hawaii,
752 USA, 8–12 November 2004, 220–227.

753 Bamberger, I., Eugster, W., Oney, B., Brunner, D., Leuenberger, M., Schanda, R., Henne, S., and
754 Buchmann, N., 2014. Tall tower or mountaintop measurements?. Geophysical Research
755 Abstracts 16, EGU2014-7169, 2014.

756 Bamberger, I., Oney, B., Brunner, D., Henne, S., Leuenberger, M., Buchmann, N., Eugster, W.,
757 2017: Observations of atmospheric methane and carbon dioxide mixing ratios: Tall-tower or
758 mountain-Top stations? Boundary Layer Meteorology, doi 10.1007/s10546-017-0236-3.

759 Cooper, O. R. and Moody, J. L. 2000. Meteorological controls on ozone at an elevated eastern
760 United States regional background monitoring site. J. Geophys. Res. 105(D5), 6855-6869.

761 Davis, K.J., Gamage, N., Hagelberg, C.R., Kiemle, C., Lenschow, D.H., Sullivan, P.P., 2000. An
762 objective method for deriving atmospheric structure from airborne lidar observations. Journal of
763 Atmospheric and Oceanic Technology 17, 1455-1468.

764 De Wekker, S.F.J., Ameen, A., Song, G., Stephens, B.B., Hallar, A.G., and McCubbin, I.B.,
765 2009. A preliminary investigation of boundary layer effects on daytime atmospheric CO₂
766 concentrations at a mountaintop location in the Rocky Mountains. Acta Geophysica 57, 904-922.

767 Desai, A.R., Helliker, B.R., Moorcroft, P.R., Andrews, A.E., and Berry, J.A., 2010. Interannual
768 variability in regional carbon fluxes from top-down and bottom-up perspectives. Journal of
769 Geophysical Research-Biogeosciences 115, G02011.

770 Dils, B., Cui, J., Henne, S., Mahieu, E., Steinbacher, M., and De Mazière, M., 2011. 1997–2007
771 CO trend at the high Alpine site Jungfraujoch: a comparison between NDIR surface in situ and
772 FTIR remote sensing observations. Atmospheric Chemistry and Physics 11, 6735-6748.

773 Draxler, R. R. and Hess, G. D. 2004. Description of the HYSPLIT 4 Modeling System (NOAA
774 Technical Memorandum ERL ARL-224). NOAA Air Resources Laboratory, Silver Spring, MD.

775 Fischer, E.V., Talbot, R.W., Dibb, J.E., Moody, J.L., and Murray, G.L., 2004. Summertime
776 ozone at Mount Washington: Meteorological controls at the highest peak in the northeast.
777 Journal of Geophysical Research 109, D24303.

778 Gao, J., Wang, T., Ding, A., and Liu, C., 2005. Observational study of ozone and carbon
779 monoxide at the summit of mount Tai (1534 m a.s.l.) in central-eastern China. Atmospheric
780 Environment 39, 4779–4791.

781 Gallagher, J.P., McKendry, I.G., Cottle, P.W., Macdonald, A.M., Leitch, W.R., and
782 Strawbridge, K., 2012. Application of lidar data to assist air mass discrimination at the Whistler
783 Mountaintop Observatory. Journal of Applied Meteorology and Climatology 51, 1733–1739.

784 Haszpra, L., Barcza, Z., Haszpra, T., Pátkai, Zs., and Davis, K.J., 2015. How well do tall tower
785 measurements characterize the CO₂ mole fraction distribution in the planetary boundary layer?,
786 Atmospheric Measurement Techniques 8, 1657-1671.

787 Henne, S., Klausen, J., Junkermann, W., Kariuki, J.M., Aseyo, J.O., Buchmann, B., 2008.
788 Representativeness and climatology of carbon monoxide and ozone at the global GAW station
789 Mt. Kenya in equatorial Africa. Atmospheric Chemistry and Physics 8, 3119-3139.

790 Justice, C. O., Giglio, L., Korontzi, S., Owens, J., Morisette, J. and co-authors. 2002. The
791 MODIS fire products. Rem. Sens. Environ. 83, 244-262.

792 Keeling, C.D., Bacastow, R.B., Bainbridge, A.E., Ekdahl, C.A.Jr., Guenther, P.R., and
793 Waterman, L.S., 1976. Atmospheric carbon-dioxide variations at Mauna-Loa Observatory,
794 Hawaii. Tellus 28 (6), 538-551.

795 [Lee, T.R., De Wekker, S.F.J., Andrews, A., Kofler, J., and Williams, J., 2012.](#) Carbon dioxide
796 variability during cold front passages and fair weather days at a forested mountaintop site.
797 *Atmospheric Environment* 46, 405-416.

798 Lee, T.R., 2015. The impact of planetary boundary layer dynamics on mountaintop trace gas
799 variability. Ph.D. dissertation, University of Virginia, 213 pp.

800 [Lee, T. R., S. F. J. De Wekker, S. Pal, A. E. Andrews, and J. Kofler, 2015.](#) Meteorological
801 controls on the diurnal variability of carbon monoxide mixing ratio at a mountaintop monitoring
802 site in the Appalachian Mountains. *Tellus B*, 67, 25659.

803 Lee, T.R., and De Wekker, S.F.J., 2016. Estimating daytime planetary boundary layer heights
804 over a valley from rawinsonde observations at a nearby airport: An application to the Page
805 Valley in Virginia, USA, *Journal of Applied Meteorology and Climatology* 55(3), 791-809.

806 Lin, J.C., Mallia, D.V., Wu, D., and Stephens, B.B., 2016. How can mountaintop CO₂
807 observations be used to constrain regional carbon fluxes?, *Atmospheric Chemistry and Physics*
808 Discussion doi:10.5194/acp-2016-762, in review, 2016.

809 [Nyeki, S., Kalberer, M., Colbeck, I., De Wekker, S.F.J., Furger, M., Gäggeler, H.W., Kossmann,](#)
810 [M., Lugauer, M., Steyn, D., Weingartner, E., Wirth, M., and Baltensperger, U., 2000.](#) Convective
811 boundary layer evolution to 4 km asl over high-alpine terrain: airborne lidar observations in the
812 Alps. *Geophysical Research Letter* 27(5), 689-692.

813 [Ou-Yang, C.-F., Lin, N.-H., Lin, C.-C., Wang, S.-H., Sheu, G.-R., Lee, C.-T., Schnell, R.C.,](#)
814 [Lang, P.M., Kawasato, T., and Wang, J.-L.](#) 2014: Characteristics of atmospheric carbon

815 monoxide at a high-mountain background station in East Asia, *Atmospheric Environment* 89,
816 613-622.

817 Pal, S , Behrendt A, Bauer H, Radlach M, Riede A, Schiller M, Wagner G and Wulfmeyer V.
818 (2008) 3 -dimensional observations of atmospheric variables during the field campaign COPS,
819 IOP Conference Series: Earth and Environmental Science 1 (1), 012031.

820 Pal, S., Behrendt, A., Wulfmeyer, V., 2010. Elastic-backscatter-lidar-based characterization of
821 the convective boundary layer and investigation of related statistics. *Annales Geophysicae* 28,
822 825-847.

823 Pal, S., 2014. Monitoring Depth of Shallow Atmospheric Boundary Layer to Complement
824 LiDAR Measurements Affected by Partial Overlap, *Remote Sensing* 6(9), 8468-8493.

825 Pal, S., Lee, T.R., Phelps, S., and De Wekker, S.F.J., 2014. Impact of atmospheric boundary
826 layer depth variability and wind reversal on the diurnal variability of aerosol concentration at a
827 valley site. *Science of the Total Environment* 496, 424-434.

828 Pal, S., Lopez, M., Schmidt, M., Ramonet, M., Xueref-Remy, I., Ciais, P., 2015. Investigation of
829 the atmospheric boundary layer height variability and its impact on the ^{222}Rn concentration over
830 a rural background site in France, *Journal of Geophysical Research-Atmospheres* 120, 623–643.

831 Pal, S., and Haeffelin, M., 2016. Forcing mechanisms governing diurnal, seasonal, and inter-
832 annual variability in the boundary layer depths: Five years of continuous lidar observations over
833 a suburban site near Paris, *Journal of Geophysical Research-Atmospheres*, DOI:
834 10.1002/2015JD023268.

835 Pillai, D., Gerbig, C., Ahmadov, R., Rödenbeck, C., Kretschmer, R., Koch, T., Thompson, R.,
836 Neining, B., and Lavrié, J.V., 2011. High-resolution simulations of atmospheric CO_2 over

837 complex terrain – representing the Ochsenkopf mountain tall tower, Atmospheric Chemistry and
838 Physics 11, 7445-7464.

839 Pino, D., Vilà-Guerau de Arellano, J., Peters, W., Schröter, J., Heerwaarden, C.C.V., Krol, M.C.,
840 2012. A conceptual framework to quantify the influence of convective boundary layer
841 development on carbon dioxide mixing ratios. Atmospheric Chemistry and Physics 12, 2969–
842 2985.

843 Popa, M. E., Gloor, M., Manning, A. C., Jordan, A., Schultz, U. and co-authors. 2010.
844 Measurements of greenhouse gases and related tracers at Bialystok tall tower station in Poland.
845 Atmos. Meas. Tech. 3, 407-427.

846 Poulida, O., Dickerson, R. R., Doddridge, B. G., Holland, J. Z., Wardell, R. G. and co-authors.
847 1991. Trace gas concentrations and meteorology in rural Virginia 1. Ozone and carbon
848 monoxide. J. Geophys. Res. 96(D12), 22461-22475.

849 Sarangi, T., Naja, M., Ojha, N., Kumar, R., Lal, S., Venkatarmani, S., Kumar, A., Sagar, R., and
850 Chandola, H.C., 2014. First simultaneous measurements of ozone, CO, and NO_y at a high-
851 altitude regional representative site in the central Himalayas. Journal of Geophysical Research-
852 Atmospheres 119, 1592-1611.

853 Steyn, D.G., De Wekker, S.F.J., Kossmann, M., and Martilli, A., 2012. Boundary Layers and Air
854 Quality in Mountainous Terrain. Chapter 5 in: Mountain Weather Research and Forecasting.
855 Recent Progress and Current Challenges. Chow, F.K., De Wekker, S.F.J., Snyder, B. (eds)
856 Springer, Berlin.

857 Sullivan, J.T., McGee, T.J., Langford, A.O., Alvarez, R.J., Senff, C.J., Reddy, P.J., Thompson,
858 A.M., Twigg, L.W., Sumnicht, G.K., Lee, P., Weinheimer, A., Knute, C., Long, R.W., and Hoff,

859 [R.M., 2016.](#), Quantifying the contribution of thermally driven recirculation to a high-ozone event
860 along the Colorado Front Range using lidar, *J. Geophys. Res. Atmos.*, 121, 10,377–10,390,
861 doi:10.1002/2016JD025229.

862 [Sullivan, J.T., Rabenhorst, S.D., Dreessen, J., McGee, T.J., Delgado, R., Twigg, L., and](#)
863 [Sumnicht, G., 2017:](#) Lidar observations revealing transport of O₃ in the presence of a nocturnal
864 low-level jet: Regional implications for “next-day” pollution, 158, 160–171.

865 [Thompson, R.L., Manning, A.C., Gloor, E., Schultz, U., Seifert, T., Hansel, F., Jordan, A., and](#)
866 [Heimann, M., 2009.](#) In-situ measurements of oxygen, carbon monoxide and greenhouse gases
867 from Ochsenkopf tall tower in Germany. *Atmospheric Measurement Techniques* 2, 573-591.

868 [Vögtlin, R., Kossmann, M., Güsten, H., Heinrich, G., Fiedler, F., Corsmeier, U., and Kalthoff,](#)
869 [N., 1996.](#) Transport of trace gases from the Upper Rhine Valley to a mountain site in the
870 Northern Black Forest. *Physics and Chemistry of the Earth* 21(5-6), 425-428.

871 [Weiss-Penzias, P., Jaffe, D.A., Swartzendruber, P., Dennison, J.B., Chand, D., Hafner, W., and](#)
872 [Prestbo, E., 2006.](#) Observations of Asian air pollution in the free troposphere at Mount Bachelor
873 Observatory during the spring of 2004. *Journal of Geophysical Research* 111, D10304.

874 [Whiteman, C.D., Bian, X., and Zhong, S. 1999.](#) Wintertime evolution of the temperature
875 inversion in the Colorado Plateau Basin. *Journal of Applied Meteorology* 38, 1103–1117.

876 [Whiteman, C.D., 2000:](#) *Mountain Meteorology: Fundamentals and Applications.* Oxford
877 University Press, 355 pages.

878 [Yi, C.X., Davis, K.J., Berger, B.W., Bakwin, P.S., 2001.](#) Long-term observations of the
879 dynamics of the continental planetary boundary layer. *Journal of Atmospheric Sciences* 58,
880 1288–1299.

881